
Mitigating Disparate Impact of Differential Privacy in Federated Learning through Robust Clustering

Saber Malekmohammadi

Mila - Quebec AI institute
School of Computer Science
University of Waterloo
Waterloo, Canada

saber.malekmohammadi@uwaterloo.ca

Afaf Taik

Mila - Quebec AI institute
Université de Montréal
Montreal, Canada
afaf.taik@mila.quebec

Golnoosh Farnadi

Mila - Quebec AI institute
McGill University
Université de Montréal
Montreal, Canada
farnadig@mila.quebec

Abstract

Federated Learning (FL) is a decentralized machine learning (ML) approach that keeps data localized and often incorporates Differential Privacy (DP) to enhance privacy guarantees. Similar to previous work on DP in ML, we observed that differentially private federated learning (DPFL) introduces performance disparities, particularly affecting minority groups. Recent work has attempted to address performance fairness in vanilla FL through clustering, but this method remains sensitive and prone to errors, which are further exacerbated by the DP noise in DPFL. To fill this gap, in this paper, we propose a novel clustered DPFL algorithm designed to effectively identify clients' clusters in highly heterogeneous settings while maintaining high accuracy with DP guarantees. To this end, we propose to cluster clients based on both their model updates and training loss values. Our proposed approach also addresses the server's uncertainties in clustering clients' model updates by employing larger batch sizes along with Gaussian Mixture Model (GMM) to alleviate the impact of noise and potential clustering errors, especially in privacy-sensitive scenarios. We provide theoretical analysis of the effectiveness of our proposed approach. We also extensively evaluate our approach across diverse data distributions and privacy budgets and show its effectiveness in mitigating the disparate impact of DP in FL settings with a small computational cost.

1 Introduction

Federated learning (FL) [1] is a collaborative machine learning (ML) paradigm allowing multiple clients to train a shared global ML model without sharing their data, and providing data privacy to clients. However, in order for FL algorithms to ensure rigorous privacy guarantees against the privacy attacks of a potentially curious server or any malicious third party [2; 3; 4; 5; 6], FL systems are reinforced with differential privacy (DP) [7; 8; 9; 10] in the presence of a trusted server (CDP) [11; 12], and in its absence (LDP) [13; 14; 15]. In LDP each client adds noise to its stochastic gradients locally and independently, which leads to a higher level of noise and more utility loss.

Given the heterogeneity of the data across different clients, how can we ensure that the model resulting from FL performs similarly for all clients? Fairness in centralized ML is usually defined Preprint. Under review.

as a notion of parity of the underlying distributions from different groups given by a protected attribute (e.g. accuracy parity [16; 17], demographic parity [18; 19] and equalized odds [20]). On the other hand, many existing works on fair FL, focus on accuracy parity across clients with one single common model [21; 22]. However, performance parity with one single model fails to capture the heterogeneity in the data quality/quantity across clients [23]. To address this, multiple methods were proposed to achieve performance parity *in non-DP FL settings*: agnostic federated learning [21], client reweighting [24; 25; 26], multi-task learning [27; 28; 29; 30], transfer learning [31; 32] and clustered FL [33] are among them. Clustered FL was proposed as an efficient personalization technique, where subsets of clients are grouped together by the server based on their loss values [34; 33; 29; 35; 30; 23], their gradients (model updates) [36; 37; 38] or their model parameters [39]. Nonetheless, as discussed in [37] in details, these approaches are prone to errors in clustering due to their sensitivity to the initial conditions and the randomness entailed by the local training. *In the case of DPFL, such vulnerability is exacerbated due to the noisy updates and resulting fluctuations in loss values.* In contrast to the existing clustering approaches, we propose a clustered DPFL algorithm based on *both* clients’ model updates and losses, making it robust to DP/stochastic noise.

Furthermore, it has been shown that DP can exacerbate existing biases in the train data and have disparate impacts on the accuracy of different subgroups of clients - even with small imbalances and loose privacy guarantees [40; 41; 42] - which is mainly due to the inequitable gradient clipping in DPSGD [42; 43; 44]. Some works proposed to use non-uniform clipping thresholds for different groups to address this tension [43; 44; 45] that has become increasingly urgent to be addressed.

Several efforts were previously made to address group fairness in CDP FL systems [46; 47]. *In contrast, we focus on mitigating the disparate impact that LDP has on accuracy across clients.* To do so, we propose a clustered DPFL algorithm, which is robust to DP/stochastic noises, and show that it successfully achieves privacy cost (excessive risk) equity [44; 45] across clients (i.e., equal LDP effect for different client groups), alongside an overall improvement in the average performance. This is achieved by using full batches during the first FL rounds to reduce the noise in clients’ model updates, which is justified by theoretical analysis. We then soft cluster clients based on these less noisy model updates using a Gaussian Mixture Model (GMM) and use the resulting clusters as an initialization for clustering clients based on their loss values in the next rounds. Our evaluations demonstrates that our proposed algorithm under various heterogeneous data distributions and different privacy budgets can cluster clients correctly with much higher chance and reduce disparities in privacy costs between the majority and minority groups. The highlights of our contributions are summarized in the following:

- We empirically demonstrate the significant impact of client batch size on the noise in their model updates.
- We theoretically prove that increasing client batch size, particularly in the initial communication round, consistently improves the server’s ability to cluster clients based on their model updates.
- We theoretically prove that sufficiently large client batch sizes, especially in the first round, enable super-linear convergence of Gaussian Mixture Model (GMM) clustering on client model updates, which leads to fast and accurate clustering.
- We propose a novel hybrid clustering algorithm that combines information from both client model updates and their loss values. This approach results in a robust and high-quality clustering solution that effectively cluster clients in highly heterogeneous settings with DP guarantees.
- Extensive evaluation across diverse and heterogeneous datasets and scenarios demonstrates the effectiveness of our robust clustered DPFL (RC-DPFL) algorithm in mitigating disparate impact and achieving results competitive with state-of-the-art DPFL.

2 Related work

Fairness in FL: As an important goal in FL, the utility of the final trained model should not vary much across clients (performance parity). For instance, [21] proposed Agnostic FL (AFL) by optimising the worst client loss function through a min-max optimization approach. TERM [25] uses tilted losses to up-weight clients with large losses. Finally, [24] and [26] proposed q -FFL and PropFair, inspired by α -fairness [48] and proportional fairness [49], respectively. Generating one common model for

all clients, these techniques do not perform well when the data distribution across clients is highly heterogeneous, leading to low overall performance in the system. Indeed, up-weighting clients with larger loss values -who might be outliers as well as adversaries- comes at the cost of the suppression of other clients who might hold large amounts of quality data.

Clustered FL has been proposed *for personalization in non-DP FL*, by hard/soft clustering clients. Assuming that clients can be naturally partitioned into clusters, existing algorithms mainly assign each client to a cluster based on its loss value [23; 29; 30; 33; 34; 35] or group clients with similar model updates (with respect to e.g. euclidean distance [37; 38] or cosine similarity [36]) into the same cluster. As stated in [37], all the existing algorithms are prone to clustering mistakes, *especially if used in DPFL systems which are affected by DP noise*, due to not rigorously checking similarity of clients throughout the training process. Clustering errors in early training rounds (due to e.g. gradient stochasticity, model initialization, or the form of loss functions far from their optima) propagate in the subsequent rounds leading to suboptimal performance. We propose an algorithm for clustering clients in FL systems with LDP, which is robust to high levels of DP/stochastic noise, and combines the above clustering strategies by clustering clients based on their model updates in the first round(s), and based on their their loss values in the next rounds.

Differential privacy and fairness: There are multiple definitions of DP. We adopt the following definition in this work:

Definition 2.1 ((ϵ, δ) -DP [8]). *A randomized mechanism $\mathcal{M} : \mathcal{D} \rightarrow \mathcal{R}$ with domain \mathcal{D} and range \mathcal{R} satisfies (ϵ, δ) -DP if for any two adjacent inputs $d, d' \in \mathcal{D}$, which differ only by a single record, and for any measurable subset of outputs $\mathcal{S} \subseteq \mathcal{R}$ it holds that*

$$\Pr[\mathcal{M}(d) \in \mathcal{S}] \leq e^\epsilon \Pr[\mathcal{M}(d') \in \mathcal{S}] + \delta.$$

In the sense of Definition 2.1, the output of an algorithm \mathcal{M} is all the information that the untrusted server observes. We consider local model of DPFL (see Figure 6 in appendix), where all clients use the same privacy parameters (ϵ, δ) , and send data-dependent computation results $\mathcal{M}(\mathcal{D}_i)$ (i.e. model updates) to the server. Also, in the context of Definition 2.1, the notion of neighboring datasets that we consider in this work, refers to pair of federated datasets $d = \{\mathcal{D}_1, \dots, \mathcal{D}_n\}$ and $d' = \{\mathcal{D}_1, \dots, \mathcal{D}_n\}$, differing by one data point of one client (i.e. *record-level* DPFL). The gaussian mechanism, which randomizes the output of a non-private computation f on a dataset d by adding an amount of noise calibrated to the sensitivity of f has been used in DPSGD algorithm [50] to achieve (ϵ, δ) -DP.

The use of DPSGD can exacerbate the unfair tendencies in models, especially for clients holding minority data points [40; 41; 42]. Some recent works tried to address this tension between group fairness and DP in centralized [43; 45] and DPFL [46; 47] settings. Close to our work, the work in [44] studied the effect of DP on the privacy cost enforced to minority data in centralized settings, and proposed a solution based on preventing gradient misalignment across different groups of data. Unlike the previous works on group fairness, [44] adopts cross-model fairness, where the cost of adding privacy to a non-private model (or excessive risk) must be fairly distributed between minority and majority groups. We adopt the same definition - which is also used in [23] - in our work, and aim to achieve it by grouping similar clients together and training a different model per cluster.

3 Notations and assumptions

We consider an FL setting with n clients. Let $x \in \mathcal{X} \subseteq \mathbb{R}^d$ and $y \in \mathcal{Y} = \{1, \dots, C\}$ denote an input data point and its target label. Client i holds dataset \mathcal{D}_i with N_i samples from distribution $P_i(x, y) = P_i(y|x)P_i(x)$. Let $h : \mathcal{X} \times \theta \rightarrow \mathbb{R}^C$ be the predictor function, which is parameterized by $\theta \in \mathbb{R}^p$. Also, let $\ell : \mathbb{R}^C \times \mathcal{Y} \rightarrow \mathbb{R}_+$ be the loss function used (cross-entropy loss). Client i in the system has empirical train loss $f_i(\theta) = \frac{1}{N_i} \sum_{(x,y) \in \mathcal{D}_i} [\ell(h(x, \theta), y)]$, with minimum value f_i^* . There are E communication rounds indexed by e , and client i runs K local epochs with learning rate η_i in round e . There are M clusters of clients indexed by m . Clients i, j belonging to the same cluster have the same data distributions ($P_i(x, y) = P_j(x, y)$), while there is data heterogeneity between clients from different clusters. We use $s(i)$ to denote the true cluster of client i and $R^e(i)$ to denote the cluster assigned by server to client i at the beginning of round e . The server holds M cluster models with parameters $\{\theta_m^e\}_{m=1}^M$ at the beginning of round $e \in [E]$. Lets assume the batch size that client i uses in the first round $e = 1$ is b_i^1 , which may be different from the batch size $b_i^{>1}$ that it uses

in the rest of the rounds $e > 1$. At the t -th gradient update during the communication round e , and given a current model θ , client i uses batch size $b_i^e = |\mathcal{B}_i^{e,t}|$, and computes the noisy batch gradient:

$$\tilde{g}_i^{e,t}(\theta) = \frac{1}{b_i^e} \left[\left(\sum_{j \in \mathcal{B}_i^{e,t}} \bar{g}_{ij}(\theta) \right) + \mathcal{N}(0, \sigma_{i,\text{DP}}^2 \mathbb{I}_p) \right], \quad (1)$$

where $\bar{g}_{ij}(\theta) = \text{clip}(\nabla \ell(h(x_{ij}, \theta), y_{ij}), c)$, c is a clipping threshold: for a given vector \mathbf{v} , $\text{clip}(\mathbf{v}, c) = \min\{\|\mathbf{v}\|, c\} \cdot \frac{\mathbf{v}}{\|\mathbf{v}\|}$. Also, \mathcal{N} is the Gaussian noise distribution with scale $\sigma_{i,\text{DP}}^2$, with $\sigma_{i,\text{DP}} = c \cdot z(\epsilon, \delta, b_i^1, b_i^{>1}, N_i, K, E)$, and z is the noise scale needed for achieving (ϵ, δ) -DP by client i , which can be determined with a privacy accountant, e.g., the moments accountant [50] used in this work. For an arbitrary random variable $\mathbf{v} = (v_1, \dots, v_p)^\top \in \mathbb{R}^{p \times 1}$, we define $\text{Var}(\mathbf{v}) := \sum_{j=1}^p \mathbb{E}[(v_j - \mathbb{E}[v_j])^2]$, i.e. variance of \mathbf{v} is the sum of the variances of its elements. Finally, we have the following assumption about batch gradients:

Assumption 3.1 (Bounded gradient variance). *The stochastic gradient $g_i^{e,t}(\theta) = \frac{1}{b_i^e} \sum_{j \in \mathcal{B}_i^{e,t}} g_{ij}(\theta)$ is an unbiased estimate of $\nabla f_i(\theta)$ with bounded variance: $\forall \theta \in \mathbb{R}^p$: $\mathbb{E}_{\mathcal{B}_i^{e,t}}[g_i^{e,t}(\theta)] = \nabla f_i(\theta)$ and $\text{Var}(g_i^{e,t}(\theta)) \leq \sigma_{i,g}^2(b_i^e)$. The tight bound $\sigma_{i,g}^2(b_i^e)$ is a constant that only depends on the used batch size b_i^e : the smaller the batch size b_i^e , the smaller the bound.*

4 Motivation, methodology and proposed algorithm

We start with the shortcomings of the existing client clustering algorithms, which give us a motivation for proposing our new approach. As discussed in [37], algorithms whose clustering strategy is based on clients' loss values [23; 29; 30; 33; 34; 35], i.e. assign client i to cluster $R(i) = \text{argmin}_m f_i(\theta_m^e) = \frac{1}{N_i} \sum_{(x,y) \in \mathcal{D}_i} \ell(h(x, \theta_m^e), y)$ at the beginning of round e , suffer from errors due to initializations of $\{\theta_m^e\}_{m=1}^M$ in the first rounds. Also, any potential clustering errors happening in the first rounds due to this reason could propagate to the end of the training. On the other hand, clustering clients based on their model updates $\{\Delta \tilde{\theta}_i^e\}_{i=1}^n$ at the end of round e , as in [37; 38], makes sense only when all clients are assigned the same model parameter at the beginning of the round e . Otherwise clients' model updates are not comparable. This condition is possible to be met only in the very first communication round $e = 1$, by initializing cluster models $\{\theta_m^e\}_{m=1}^M$ with the same model parameter θ^{init} . However, due to assigning clients to different clusters, this is not possible in the next rounds ($e > 1$). Hence, as opposed to what done in [38] and in an example in [37], clustering clients based on $\{\Delta \tilde{\theta}_i^e\}_{i=1}^n$ does not fully make sense for $e \geq 2$.

In the following, we propose to cluster clients based on their model updates at the end of the first round $e = 1$ ($\forall m \in [M] : \theta_m^1 = \theta^{\text{init}}$), and based on their loss values in the subsequent rounds.

4.1 RC-DPFL algorithm

Following the analysis of the previous clustered FL algorithms, we introduce robust clustered DPFL (RC-DPFL) algorithm, reported in Algorithm 1, which has the following three main stages:

round ($e = 1$): The server initializes all cluster models equally ($\forall m \in [M] : \theta_m^1 = \theta^{\text{init}}$), and clients perform local training on this common model with full batch size $b_i^1 = N_i$. In Section 4.2, we analyze the effect of the batch size on the clustering quality, and in Section 4.2.3 we analyze the convergence rate of the GMM algorithm in these conditions. Note that even when clients have limited memory budget, they can still perform DPSGD with full batch size using gradinet accumulation technique (see Appendix E). At the end of the round, the server clusters the clients' noisy model updates using GMM soft clustering algorithm returning soft clustering $\pi_i \in \mathbb{R}^M$ for each client i .

rounds $e \in \{2, \dots, E_c\}$: we continue training with the output of the GMM clustering for the next rounds $E_c - 1$ rounds. During these rounds the uncertainties in clustering of clients in the first round is incorporated in the probabilities returned by GMM: client i contributes to the training of each cluster (m) model proportional to the probability of its assignment to that cluster ($\pi_{i,m}$).

rounds $e \in \{E_c + 1, \dots, E\}$: After the first E_c rounds, some progress has been made in the training of the cluster models $\{\theta_m^e\}_{m=1}^M$, and we can change the clustering strategy to clients losses. More specifically, at the end of round $e \geq E_c + 1$, client i is assigned to cluster $R(i) = \text{argmin}_m f_i(\theta_m^e) = \frac{1}{N_i} \sum_{(x,y) \in \mathcal{D}_i} \ell(h(x, \theta_m^e), y)$, i.e. the cluster model with the lowest loss on the client's train data.

4.2 Reducing clustering uncertainty via larger batch size

4.2.1 Effect of batch size on clients' DP noisy model updates

As observed in Equation (1), performing DPSGD by clients locally makes their model updates noisy and causes their training losses to fluctuate. As such, our client clustering method should address this noise. In the following, we first show that the noise in client i 's model update at the of round e , including stochastic and DP noise, heavily depends on the batch size b_i^e used by the client during that round. These findings will lead us to the design of our robust clustering algorithm.

Lemma 4.1. *Using the notations in Section 3, lets assume $\theta_{i,0}^e$ is the model parameter that is passed by the server to client i at the beginning of the round e , and it performs K local epochs of DPSGD on its local data \mathcal{D}_i with batch size b_i^e to generate the noisy DP model update $\Delta\tilde{\theta}_i^e(b_i^e)$. Assuming that the clipping threshold c is effective for all sampled data points in the batch, i.e. $\forall j \in \mathcal{B}_i^{e,t} : c < \|g_{ij}(\theta)\| = \|\nabla\ell(h(x_{ij}, \theta), y_{ij})\|$, we have:*

$$\sigma_i^{e,2}(b_i^e) := \text{Var}(\Delta\tilde{\theta}_i^e(b_i^e)|\theta_{i,0}^e) \approx K \cdot N_i \cdot \eta_l^2 \cdot \frac{pc^2z^2(\epsilon, \delta, b_i^1, b_i^{>1}, N_i, K, E)}{b_i^{e,3}}. \quad (2)$$

Note that the assumption of having a clipping threshold effective for all data samples is reasonable, especially in the first round that clients losses are relatively large, as we avoid adding unnecessary DP noise by avoiding large and ineffective clipping thresholds c . This means that $\sigma_i^{e,2}$ heavily depends on b_i^e , as it appears with power 3 in denominator. Hence, $\sigma_i^{e,2}$, or equivalently the noise in $\Delta\tilde{\theta}_i^e(b_i^e)$, decreases rapidly as b_i^e increases. We show b_i^e as an argument of $\sigma_i^{e,2}$ to insist on its dependence on b_i^e .

4.2.2 Effect of batch sizes $\{b_i^1\}_{i=1}^n$ on model updates $\{\Delta\tilde{\theta}_i^1\}_{i=1}^n$

In this section, we focus on round $e = 1$, and show theoretically that increasing batch sizes $\{b_i^1\}_{i=1}^n$ (the batch sizes used by clients during the first round) improves the distinguishability of the model updates $\{\Delta\tilde{\theta}_i^1\}_{i=1}^n$ by the server. *For simplicity, throughout this section, we assume clients have the same dataset sizes $N_i = N$.* Also, let's also assume that $\forall i : \theta_{i,0}^1 = \theta^{init}$, $b_i^1 = b^1$, i.e. in the first round $e = 1$, all clients start with the same model parameter θ^{init} , and use the same batch size b^1 . According to Equation (2) and having uniform privacy parameters (ϵ, δ) , we have: $\forall i : \sigma_i^{1,2}(b^1) = \text{Var}(\Delta\tilde{\theta}_i^1(b^1)|\theta^{init}) = \sigma^{1,2}(b^1)$. Hence, we can consider the model updates $\{\Delta\tilde{\theta}_i^1\}_{i=1}^n$ as the samples from a mixture of M Gaussian distributions with parameters (mean, covariance matrix, prior probability) $\psi^*(b^1) = \{(\mu_m^*(b^1), \Sigma_m^*(b^1), \alpha_m^*)\}_{m=1}^M$, where $\mu_m^*(b^1) \neq \mu_{m'}^*(b^1)$ ($m \neq m'$) due to data heterogeneity across clusters and the model update $\Delta\tilde{\theta}_i^1$ comes from the Gaussian component $m = s(i)$. Note that $\{(\mu_m^*(b^1), \Sigma_m^*(b^1))\}_{m=1}^M$ vary when b^1 changes:

$$\mu_m^*(b^1) = \mathbb{E} \left[\Delta\tilde{\theta}_i^1(b_i^1) \middle| \theta^{init}, b_i^1 = b^1, s(i) = m \right], \quad (3)$$

$$\Sigma_m^*(b^1) = \mathbb{E} \left[(\Delta\tilde{\theta}_i^1(b_i^1) - \mu_m^*(b^1)) (\Delta\tilde{\theta}_i^1(b_i^1) - \mu_m^*(b^1))^\top \middle| \theta^{init}, b_i^1 = b^1, s(i) = m \right] = \frac{\sigma^{1,2}(b^1)}{p} \mathbb{I}_p, \quad (4)$$

where the last line is from $\text{Var}(\Delta\tilde{\theta}_i^1|\theta^{init}, b_i^1 = b^1) = \mathbb{E}[\|\Delta\tilde{\theta}_i^1 - \mu_{s(i)}^*(b^1)\|^2] = \sigma_i^{1,2}(b^1) = \sigma^{1,2}(b^1)$ and that the noises existing in each of the p elements of $\Delta\tilde{\theta}_i^1$ are *iid* (hence, diagonal covariance matrix with equal diagonal elements). Intuitively, we expect that more separation between the true Gaussian components $\{\mathcal{N}(\mu_m^*(b^1), \Sigma_m^*(b^1))\}_{m=1}^M$, from which clients' model updates $\{\Delta\tilde{\theta}_i^1\}_{i=1}^n$ are sampled, makes the model updates more distinguishable for the server, i.e. easier for it to cluster them. In the following, we show that this is indeed the case and the overlap between the true components $\{\mathcal{N}(\mu_m^*(b^1), \Sigma_m^*(b^1))\}_{m=1}^M$ decreases fast with the increment of batch size b^1 .

Lemma 4.2. *Using the notations above, let's assume $\Delta_{m,m'}(b^1) := \|\mu_m^*(b^1) - \mu_{m'}^*(b^1)\|$ when $\forall i : b_i^1 = b^1$ (m and m' are two of the M Gaussian components). Then, the overlap between the*

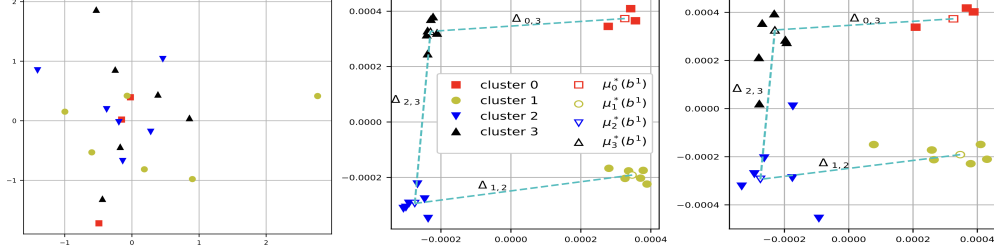


Figure 1: 2D visualization of model updates $\{\Delta\tilde{\theta}_i^1\}_{i=1}^n$ on CIFAR10 with covariate shift (rotation). **Left:** $\epsilon_i = 10$, DPFedAvg with $b_i^e = 32$ for all i, e **Middle:** $\epsilon_i = 10$, $b_i^1 = b^1 = N$ for all i , and $b_i^e = 32$ for all i and $e > 1$ **Right:** $\epsilon_i = 4$, $b_i^1 = b^1 = N$ for all i , and $b_i^e = 32$ for all i and $e > 1$.

pair of corresponding true Gaussian components $\mathcal{N}(\mu_m^*(b^1), \Sigma_m^*(b^1))$ and $\mathcal{N}(\mu_{m'}^*(b^1), \Sigma_{m'}^*(b^1))$ is $2Q\left(\frac{\sqrt{p}\Delta_{m,m'}(b^1)}{2\sigma^1(b^1)}\right)$, where $\sigma^1(b^1) = \text{Var}(\Delta\tilde{\theta}_i^1 | \theta^{\text{init}}, b_i^1 = b^1)$ and $Q(\cdot)$ is the tail distribution function of the standard normal distribution. Furthermore, if we increase $b_i^1 = b^1$ to $b_i^1 = kb^1$ (for all i), the overlap between the corresponding components m and m' drops to $2Q\left(\frac{\sqrt{kp}\Delta_{m,m'}(b^1)}{2\sigma^1(b^1)}\right)$.

The lemma above states that, assuming that the underlying Gaussian components have a separation due to data heterogeneity across clients, then using large batch size in the first round results in fast reduction of the overlap between the underlying components. Consequently, the clients' model updates $\{\Delta\tilde{\theta}_i^1\}_{i=1}^n$, which are sampled from them will also be easier to distinguish for the server. Note that, according to Equation (2), $\sigma^1(b^1)$ depends on the privacy parameter ϵ too. Hence, as clients become more privacy sensitive, the overlap increases and leads to harder clustering of clients' model updates by server (compare Figure 1 middle and right, for an illustration of this effect).

4.2.3 Convergence rate of the server GMM clustering in round $e = 1$

Lets still assume that $b_i^1 = b^1$ for all i , and that GMM clustering of $\{\Delta\tilde{\theta}_i^1(b^1)\}_{i=1}^n$ by server converges to a local optimum $\{(\mu_m(b^1), \Sigma_m(b^1), \alpha_m(b^1))\}_{m=1}^M$ (EM objective function is non-convex). If the batch size b^1 is large enough, and the number of model updates (samples) $\{\Delta\tilde{\theta}_i^1(b^1)\}_{i=1}^n$ is large, we expect GMM clustering of the model updates to converge to the true parameters $\psi^*(b^1) = \{(\mu_m^*(b^1), \Sigma_m^*(b^1), \alpha_m^*)\}_{m=1}^M$. Assuming that this is the case, we analyze the local convergence rate of GMM around this true solution $\psi^*(b^1)$. We define $O(\psi^*(b^1)) = \max_{m,m'} O_{m,m'}(\psi^*(b^1))$, as the maximum pairwise overlap between the true Gaussian components. We now consider some assumptions, regularizing the way $O(\psi^*(b^1))$ tends to zero as b^1 increases (based on Lemma 4.2).

conditions 1: $\alpha_m^* \geq \alpha$, $m \in \{1, 2, \dots, M\}$, where α is a positive number. In other words, the prior probabilities of all the M Gaussian components remain non-zero.

conditions 2: $\forall m, m' : \nu D_{\max}(\psi^*(b^1)) \leq D_{\min}(\psi^*(b^1)) \leq \|\mu_m^*(b^1) - \mu_{m'}^*(b^1)\| \leq D_{\max}(\psi^*(b^1))$, where ν is a positive number. It means that the pairwise distance between mean vectors $\{\mu_m^*(b^1)\}_{m=1}^M$ are of the same order and no pair completely overlap as b^1 grows.

Both the conditions above are satisfied in our setting, as we assume we have M different clusters with heterogeneous data distributions, which make $\{\mu_m^*(b^1)\}_{m=1}^M$ different for all b^1 . Then, we have:

Theorem 4.3. ([51]) Given iid model updates $\{\Delta\tilde{\theta}_i^1(b^1)\}_{i=1}^n$ sampled from the mixture of Gaussians $\{\mathcal{N}(\mu_m^*(b^1), \Sigma_m^*(b^1)), \alpha_m^*\}_{m=1}^M$ that satisfies conditions 1 and 2, as b^1 grows. If b^1 grows enough that $O(\psi^*(b^1))$ is considered as an infinitesimal, we have:

$$\lim_{r \rightarrow \infty} \frac{\|\psi^{r+1} - \psi^*(b^1)\|}{\|\psi^r - \psi^*(b^1)\|} = o(O(\psi^*(b^1))^{0.5-\epsilon}), \quad (5)$$

as n grows, where ψ^r is the mixture model parameters returned by GMM after r iterations. ϵ is an arbitrary small positive number, and $o(x)$ means it is a higher order infinitesimal as $x \rightarrow 0$.

This means that convergence rate of GMM clustering of clients' model updates around the true solution $\psi^*(b^1)$, which is achievable by running EM when b^1 grows enough, is a higher order in-

Algorithm 1: RC-DPFL

Input: Initial parameter θ^{init} , number of clusters M , batch sizes b , dataset sizes $\{N_1, \dots, N_n\}$, noise scales $\{z_1, \dots, z_n\}$, gradient norm bound c , local epochs K , global round E .
Output: $\theta^E, \{\epsilon_1^E, \dots, \epsilon_n^E\}$

```
1 Initialize  $\theta_1^1 = \dots = \theta_m^1 = \theta^{init}$ ; // avoid potential errors due to different
   model initializations
2 for  $e \in \{1, \dots, E_c\}$  do
3   if  $e = 1$  then
4     for each client  $i \in \{1, \dots, n\}$  in parallel do
5        $b_i^e \leftarrow N_i$ ; // full batch
6        $\Delta \tilde{\theta}_i^e \leftarrow \text{DPSGD}(\theta_1^e, b_i, N_i, K, z_i, c)$ 
7        $\{\pi_1, \dots, \pi_n\} = \text{GMM}(\Delta \tilde{\theta}_1^e, \dots, \Delta \tilde{\theta}_n^e; M)$ ; // vector  $\pi_i \in \mathbb{R}^M$  for client  $i$ 
8       for  $i \in \{1, \dots, n\}$  do
9          $R^{e+1}(i) \leftarrow m$  with probability  $\pi_i[m]$ ; // sample from GMM output
10    else if  $e \in \{2, \dots, E\}$  then
11      for each client  $i \in \{1, \dots, n\}$  in parallel do
12         $b_i^e \leftarrow b$ ; // back to normal batch size  $b$ 
13         $\Delta \tilde{\theta}_i^e \leftarrow \text{DPSGD}(\theta_{R^e(i)}^e, b_i^e, N_i, K, z_i, c)$ ; // client  $i$  is assigned  $\theta_{R^e(i)}^e$ 
14         $w_i^e \leftarrow \frac{N_i}{\sum_{j=1}^n \mathbb{1}_{R^e(j)=R^e(i)} N_j}$ 
15      for  $m \in \{1, \dots, M\}$  do
16         $\theta_m^{e+1} \leftarrow \theta_m^e + \sum_{i \in \{1, \dots, n\}} \mathbb{1}_{R^e(i)=m} w_i^e \Delta \tilde{\theta}_i^e$ ; // client  $i$  contributes to
           model  $R^e(i)$  at the end of round  $e$ 
17      if  $e \in \{2, \dots, E_c\}$  then
18        for  $i \in \{1, \dots, n\}$  do
19           $R^{e+1}(i) \leftarrow m$  with probability  $\pi_i[m]$ ; // sample from GMM output
20      else if  $e \in \{E_c + 1, \dots, E\}$  then
21        for  $i \in \{1, \dots, n\}$  do
22           $R^{e+1}(i) = \text{argmin}_m f_i(\theta_m^{e+1}) = \frac{1}{N_i} \sum_{(x,y) \in \mathcal{D}_i} [\ell(h(x, \theta_m^{e+1}), y)]$ ; // change
           the clustering strategy to be based on loss values
```

finitesimal of $O(\psi^*(b^1))^{0.5-\epsilon}$. In other words, convergence rate of *GMM* approaches approximately 0 when b^1 increases enough.

4.3 Applicability of RC-DPFL

Based on the findings in the previous section, and that $b_i^1 \leq N_i$, a question that rises about RC-DPFL is that what if the local dataset size (N_i) of some or all clients are not large enough so that using full batch size will result in enough separation between the model updates of clients from different clusters? Let's get back to Equation (1) again. Assuming having image data, if we assume we augment the local dataset of each client by adding moderate perturbations of each image $\tau - 1$ times, the local dataset size gets τ times larger. In this case, because of the repetitions of each image and its perturbations τ times, the sensitivity of the batch gradient $\frac{1}{b_i^e} \left(\sum_{j \in \mathcal{B}_i^{e,t}} \bar{g}_{ij}(\theta) \right)$ to each actual image increases to $\frac{\tau c}{b_i^e}$, as opposed to $\frac{c}{b_i^e}$ before the augmentation. This leads to τ^2 times increment in the DP noise variance $\sigma_{i,\text{DP}}^2$, which makes it inapplicable. Some solutions have been proposed for keeping the sensitivity low even after augmentation, e.g. leveraging the benefits of data augmentation by averaging per-example gradients across multiple augmentations of the same image before the clipping operation [52]. However, this idea leads to the same upper bound N_i on the batch size of client i . However, if we use data augmentation and also use full batch size i.e. $b^e = \tau N_i$, then the sensitivity of the batch gradient with respect to each image and its augmentations would be $\frac{\tau c}{b^e} = \frac{c}{N_i}$, i.e. the same sensitivity before the augmentation. *Therefore, in RC-DPFL, clients always use full batch size in the first round, and also use data augmentation if needed (i.e., for $O(\psi^*(b^1))$ to decrease sufficiently).*

5 Evaluation

Experimental Setup:

Datasets, models and baseline algorithms: We evaluate our proposed method on three benchmark datasets, including: MNIST [53], FMNIST [54] and CIFAR10 [55], with heterogeneous data distributions from covariate shift (rotation) [56; 37] and concept shift (label flip) [37] (see Appendix A). We consider four clusters of clients indexed by $m \in \{0, 1, 2, 3\}$ with $\{3, 6, 6, 6\}$ clients, respectively. Also, we compare four baseline algorithms: 1. DPFedAvg [57]: clients run DPSGD locally and send their model updates to the server for aggregation 2. KM-CDPFL [37]: FL with myopic clustering, in which server clusters clients at the end of each round using running KM++ on their model updates 3. f-CDPFL [34; 33]: FL with loss clustering, which clusters clients just based on their train loss values with different cluster models 4. O-CDPFL: an oracle algorithm which has the knowledge of true clusters from the first round.

Evaluation metrics and baselines: Fairness of a DPFL system can be measured in terms of the disparate impact of DP on different groups [23; 42; 58; 44]. Given the set of clients $i \in \{1, \dots, n\}$, the overall fairness score among them can be determined based on the privacy cost that they pay in terms of their accuracy [42] or their train loss [58; 44; 23]: $\mathcal{F}_{acc}(\{\theta_i\}_{i \in [n]}) = \max_{i,j \in [n]} |\Delta acc_i(\theta_i) - \Delta acc_j(\theta_j)|$ and $\mathcal{F}_{loss}(\{\theta_i\}_{i \in [n]}) = \max_{i,j \in [n]} |\xi_i(\theta_i) - \xi_j(\theta_j)|$ where θ_i is the model assigned to agent i at the end of DP training. $\Delta acc_i(\theta_i) = \max_{\theta^*} acc_i(\theta^*) - acc_i(\theta_i)$, and $\xi_i(\theta_i) = f_i(\theta_i) - \min_{\theta^*} f_i(\theta^*)$, where θ^* is any possible model. Following [23], we estimate the model θ^* for each cluster by centrally training a model with SGD based on the data of the clients belonging to that cluster. These notions of fairness compares the cost of privacy on different clients, and define client-level fairness as the equality of “privacy cost” across clients. We also consider the following evaluation metrics: average test accuracy (overall, majority, minority), worst accuracy across clients [21], and maximum accuracy disparity across clients: $\max_{i,j} |acc_i(\theta_i) - acc_j(\theta_j)|$.

Results: In our experiments, we aim to 1) compare RC-DPFL with other clustering approaches, 2) analyze its robustness to noise; and 3) evaluate its robustness to different types of client heterogeneity. As a result, we answer the following research questions:

RQ1: How does RC-DPFL perform compared to other algorithms? We first explore how RC-DPFL performs in comparison with the defined baseline algorithms. Figure 2 shows the performance for MNIST and FMNIST in terms of per cluster performance and privacy cost fairness. Through these results, it is clear that RC-DPFL performance on-par with the oracle-DPFL baseline, which constitutes the ideal case. This is mainly attributed to the accurate clustering obtained in RC-DPFL as seen in subfigure (c), which compares the success rate of clustering using loss function (f-CDPFL) versus our approach. KM-CDPFL, which is the least performing, also incurs the highest disparity in privacy cost.

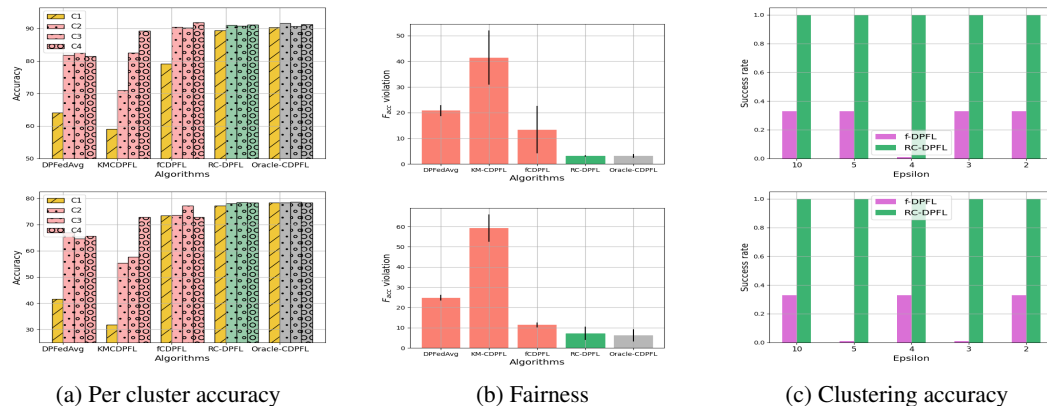


Figure 2: Comparison of RC-DPFL with the defined baselines on MNIST (Top row) and FMNIST (bottom row) with C1 being the minority cluster. All results are for $\epsilon = 5$.

RQ2: How does RC-DPFL perform under different levels of noise? Figure 3 shows how the clustering algorithms perform under varying levels of noise. Results on MNIST and FMNIST show

that KM-CDPFL is more sensitive to noise compared to f-CDPFL and RC-DPFL, with the disparity becoming more pronounced with higher noise levels (i.e., smaller *epsilon* values). RC-DPFL has the smallest gap between majority and minority groups in the majority of the experiments and outperforms the two other algorithms for minority groups in all the experiments. Detailed results can be found in Table 4, Table 3, Table 6, Table 5, Table 8 Table 7 in the appendix, which include results for various fairness metrics and accuracy across groups with varying noise levels.

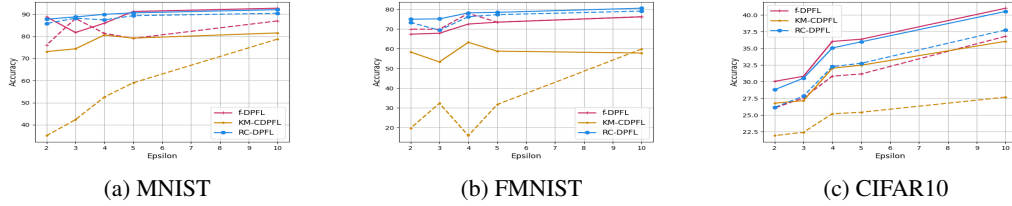


Figure 3: Effect of ϵ values on the accuracy for minority (dashed lines) and majority (solid lines) groups.

RQ3: How does RC-DPFL perform under different types of data heterogeneity across clients?

We evaluate how different types of distribution shift across client groups affect the clustered DPFL algorithms. To do so, we compare covariate shift and concept shift on CIFAR10 dataset. Concept shift, which can also be viewed as a label flipping attack, has a more significant impact on performance in the single model case, as labels vary across client groups. Figure 4 shows results with $\epsilon = 5.0$ in terms of per-cluster performance and fairness, as well as clustering accuracy for different values of ϵ . Through these results, we notice that it is easier to detect minorities with the loss values in the case of concept-shift. Nonetheless, we also note that mistakes become more costly in this case. Table 10, Table 9 in the appendix show a high variance for f-CPFL across experiments, especially smaller values of ϵ , while RC-DPFL is more consistent. Additionally, in terms of fairness metrics, and across different ϵ values, RC-DPFL still outperforms the baselines, and remains closer to the oracle case.

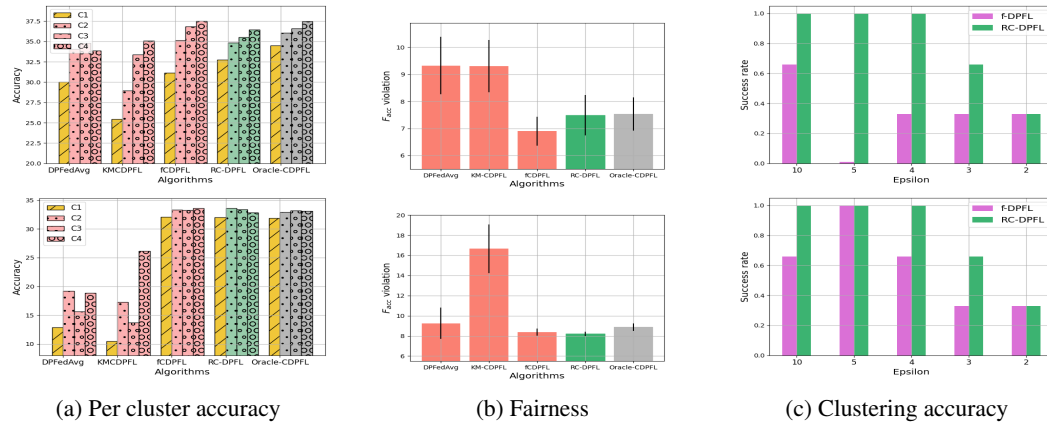


Figure 4: Comparison of RC-DPFL with the defined baselines on CIFAR10 with covariate shift (Top row) and concept-shift (bottom row) with C1 being the minority cluster. All results are for $\epsilon = 5$.

6 Conclusion

In conclusion, our novel RC-DPFL algorithm addresses performance disparities in privacy-sensitive FL environments. This is achieved through effectively identifying client clusters in highly heterogeneous settings. By clustering clients based on their model updates and training loss values, and mitigating noise impacts with larger batch sizes, our approach enhances accuracy while maintaining DP guarantees. Extensive evaluations demonstrate the effectiveness of our method in reducing the disparate impact of DP in FL settings, with minimal computational overhead.

Broader impact: Our work reconciles fairness and privacy in decentralized ML, making it more appealing to adopt in heterogeneous FL settings. Moreover, the robustness to noise, and the ability to handle various types of distribution shift makes our approach applicable to adversarial settings.

Limitations and future work: Our work relies on the assumption that the number of separable clusters is known, which is applicable in cases where demographic groups for instance are known to have varying performance (e.g., voice recognition [59]). However, techniques to determine the number of clusters in the case of DPFL would enable our approach to be more widely adopted.

Acknowledgement

Funding support for project activities has been partially provided by Canada CIFAR AI Chair, Facebook award, Google award, and MEI award. We also express our gratitude to Compute Canada for their support in providing facilities for our evaluations.

References

- [1] Brendan McMahan, Eider Moore, Daniel Ramage, Seth Hampson, and Blaise Aguera y Arcas. Communication-efficient learning of deep networks from decentralized data. In *Artificial intelligence and statistics*, pages 1273–1282. PMLR, 2017.
- [2] Briland Hitaj, Giuseppe Ateniese, and Fernando Pérez-Cruz. Deep models under the gan: Information leakage from collaborative deep learning. *Proceedings of the 2017 ACM SIGSAC Conference on Computer and Communications Security*, 2017.
- [3] Maria Rigaki and Sebastián García. A survey of privacy attacks in machine learning. *ArXiv*, 2020.
- [4] Zhibo Wang, Mengkai Song, Zhifei Zhang, Yang Song, Qian Wang, and Hairong Qi. Beyond inferring class representatives: User-level privacy leakage from federated learning. *IEEE INFOCOM*, 2019.
- [5] Ligeng Zhu, Zhijian Liu, and Song Han. Deep leakage from gradients. In *Neural Information Processing Systems*, 2019.
- [6] Jonas Geiping, Hartmut Bauermeister, Hannah Dröge, and Michael Moeller. Inverting gradients - how easy is it to break privacy in federated learning? *ArXiv*, 2020.
- [7] Cynthia Dwork, Frank McSherry, Kobbi Nissim, and Adam Smith. Calibrating noise to sensitivity in private data analysis. In *Proceedings of the Third Conference on Theory of Cryptography*. Springer-Verlag, 2006.
- [8] Cynthia Dwork, Krishnaram Kenthapadi, Frank McSherry, Ilya Mironov, and Moni Naor. Our data, ourselves: Privacy via distributed noise generation. In *Proceedings of the 24th Annual International Conference on The Theory and Applications of Cryptographic Techniques*, 2006.
- [9] Cynthia Dwork. A firm foundation for private data analysis. *Commun. ACM*, 2011.
- [10] Cynthia Dwork and Aaron Roth. The algorithmic foundations of differential privacy. *Found. Trends Theor. Comput. Sci.*, 2014.
- [11] H. Brendan McMahan, Daniel Ramage, Kunal Talwar, and Li Zhang. Learning differentially private recurrent language models. In *ICLR*, 2018.
- [12] Robin C. Geyer, Tassilo Klein, and Moin Nabi. Differentially private federated learning: A client level perspective. *ArXiv*, 2017.
- [13] Yang Zhao, Jun Zhao, Mengmeng Yang, Teng Wang, Ning Wang, Lingjuan Lyu, Dusit Tao Niyato, and Kwok-Yan Lam. Local differential privacy-based federated learning for internet of things. *IEEE Internet of Things Journal*, 8:8836–8853, 2020.
- [14] John C. Duchi, Michael I. Jordan, and Martin J. Wainwright. Local privacy and statistical minimax rates. *2013 51st Annual Allerton Conference on Communication, Control, and Computing (Allerton)*, pages 1592–1592, 2013.
- [15] John C. Duchi, Martin J. Wainwright, and Michael I. Jordan. Minimax optimal procedures for locally private estimation. *Journal of the American Statistical Association*, 113:182 – 201, 2018.
- [16] Joy Buolamwini and Timnit Gebru. Gender shades: Intersectional accuracy disparities in commercial gender classification. In Sorelle A. Friedler and Christo Wilson, editors, *Proceedings of the 1st Conference on Fairness, Accountability and Transparency*, volume 81 of *Proceedings of Machine Learning Research*, pages 77–91. PMLR, 23–24 Feb 2018.
- [17] Han Zhao and Geoff Gordon. Inherent tradeoffs in learning fair representations. In H. Wallach, H. Larochelle, A. Beygelzimer, F. d'Alché-Buc, E. Fox, and R. Garnett, editors, *Advances in Neural Information Processing Systems*, volume 32. Curran Associates, Inc., 2019.

- [18] Cynthia Dwork, Moritz Hardt, Toniann Pitassi, Omer Reingold, and Richard Zemel. Fairness through awareness. In *Proceedings of the 3rd Innovations in Theoretical Computer Science Conference*, ITCS '12, page 214–226, New York, NY, USA, 2012. Association for Computing Machinery.
- [19] Rich Zemel, Yu Wu, Kevin Swersky, Toni Pitassi, and Cynthia Dwork. Learning fair representations. In Sanjoy Dasgupta and David McAllester, editors, *Proceedings of the 30th International Conference on Machine Learning*, volume 28 of *Proceedings of Machine Learning Research*, pages 325–333, Atlanta, Georgia, USA, 17–19 Jun 2013. PMLR.
- [20] Moritz Hardt, Eric Price, Eric Price, and Nati Srebro. Equality of opportunity in supervised learning. In D. Lee, M. Sugiyama, U. Luxburg, I. Guyon, and R. Garnett, editors, *Advances in Neural Information Processing Systems*, volume 29. Curran Associates, Inc., 2016.
- [21] Mehryar Mohri, Gary Sivek, and Ananda Theertha Suresh. Agnostic federated learning. In *International Conference on Machine Learning*, pages 4615–4625. PMLR, 2019.
- [22] Umberto Michieli and Mete Ozay. Are all users treated fairly in federated learning systems? In *Proceedings of the IEEE/CVF Conference on Computer Vision and Pattern Recognition*, pages 2318–2322, 2021.
- [23] Wenda Chu, Chulin Xie, Boxin Wang, Linyi Li, Lang Yin, Arash Nourian, Han Zhao, and Bo Li. Focus: Fairness via agent-awareness for federated learning on heterogeneous data, 2023.
- [24] Tian Li, Maziar Sanjabi, Ahmad Beirami, and Virginia Smith. Fair resource allocation in federated learning. In *International Conference on Learning Representations*, 2020.
- [25] Tian Li, Ahmad Beirami, Maziar Sanjabi, and Virginia Smith. Tilted empirical risk minimization. In *International Conference on Learning Representations*, 2020.
- [26] Guojun Zhang, Saber Malekmohammadi, Xi Chen, and Yaoliang Yu. Proportional fairness in federated learning. *Transactions on Machine Learning Research*, 2023.
- [27] Virginia Smith, Chao-Kai Chiang, Maziar Sanjabi, and Ameet Talwalkar. Federated multi-task learning. In *Neural Information Processing Systems*, 2017.
- [28] Tian Li, Shengyuan Hu, Ahmad Beirami, and Virginia Smith. Ditto: Fair and robust federated learning through personalization. In Marina Meila and Tong Zhang, editors, *Proceedings of the 38th International Conference on Machine Learning*, volume 139 of *Proceedings of Machine Learning Research*, pages 6357–6368. PMLR, 18–24 Jul 2021.
- [29] Othmane Marfoq, Giovanni Neglia, Aurélien Bellet, Laetitia Kamani, and Richard Vidal. Federated multi-task learning under a mixture of distributions. In *Neural Information Processing Systems*, 2021.
- [30] Yue Wu, Shuaicheng Zhang, Wenchao Yu, Yanchi Liu, Quanquan Gu, Dawei Zhou, Haifeng Chen, and Wei Cheng. Personalized federated learning under mixture of distributions. *ArXiv*, abs/2305.01068, 2023.
- [31] Daliang Li and Junpu Wang. Fedmd: Heterogenous federated learning via model distillation. *ArXiv*, abs/1910.03581, 2019.
- [32] Yang Liu, Yan Kang, Chaoping Xing, Tianjian Chen, and Qiang Yang. A secure federated transfer learning framework. *IEEE Intelligent Systems*, 35:70–82, 2020.
- [33] Yishay Mansour, Mehryar Mohri, Jae Ro, and Ananda Theertha Suresh. Three approaches for personalization with applications to federated learning, 2020.
- [34] Avishek Ghosh, Jichan Chung, Dong Yin, and Kannan Ramchandran. An efficient framework for clustered federated learning. In H. Larochelle, M. Ranzato, R. Hadsell, M.F. Balcan, and H. Lin, editors, *Advances in Neural Information Processing Systems*, volume 33, pages 19586–19597. Curran Associates, Inc., 2020.
- [35] Yichen Ruan and Carlee Joe-Wong. Fedsoft: Soft clustered federated learning with proximal local updating. *CoRR*, abs/2112.06053, 2021.

- [36] Felix Sattler, Klaus-Robert Müller, and Wojciech Samek. Clustered federated learning: Model-agnostic distributed multitask optimization under privacy constraints. *IEEE Transactions on Neural Networks and Learning Systems*, 32:3710–3722, 2019.
- [37] Mariel Werner, Lie He, Sai Praneeth Karimireddy, Michael Jordan, and Martin Jaggi. Provably personalized and robust federated learning, 2023.
- [38] Christopher Briggs, Zhong Fan, and Peter Andras. Federated learning with hierarchical clustering of local updates to improve training on non-iid data, 2020.
- [39] Ming Xie, Guodong Long, Tao Shen, Tianyi Zhou, Xianzhi Wang, and Jing Jiang. Multi-center federated learning. *CoRR*, abs/2005.01026, 2020.
- [40] Tom Farrand, FatemehSadat Mireshghallah, Sahib Singh, and Andrew Trask. Neither private nor fair: Impact of data imbalance on utility and fairness in differential privacy. *Proceedings of the 2020 Workshop on Privacy-Preserving Machine Learning in Practice*, 2020.
- [41] Ferdinando Fioretto, Cuong Tran, Pascal Van Hentenryck, and Keyu Zhu. Differential privacy and fairness in decisions and learning tasks: A survey. In *Proceedings of the Thirty-First International Joint Conference on Artificial Intelligence*. International Joint Conferences on Artificial Intelligence Organization, jul 2022.
- [42] Eugene Bagdasaryan and Vitaly Shmatikov. Differential privacy has disparate impact on model accuracy. In *Neural Information Processing Systems*, 2019.
- [43] Depeng Xu, Wei Du, and Xintao Wu. Removing disparate impact on model accuracy in differentially private stochastic gradient descent. *Proceedings of the 27th ACM SIGKDD Conference on Knowledge Discovery & Data Mining*, 2021.
- [44] Maria S. Esipova, Atiyeh Ashari Ghomi, Yaqiao Luo, and Jesse C. Cresswell. Disparate impact in differential privacy from gradient misalignment. *ArXiv*, abs/2206.07737, 2022.
- [45] Cuong Tran, Ferdinando Fioretto, and Pascal Van Hentenryck. Differentially private and fair deep learning: A lagrangian dual approach. *ArXiv*, abs/2009.12562, 2020.
- [46] Sikha Pentylala, Nicola Neophytou, Anderson Nascimento, Martine De Cock, and Golnoosh Farnadi. Privfairfl: Privacy-preserving group fairness in federated learning, 2022.
- [47] Borja Rodr'iguez G'alvez, Filip Granqvist, Rogier C. van Dalen, and Matthew Stephen Seigel. Enforcing fairness in private federated learning via the modified method of differential multipliers. *ArXiv*, abs/2109.08604, 2021.
- [48] Tian Lan, David Kao, Mung Chiang, and Ashutosh Sabharwal. An axiomatic theory of fairness in network resource allocation. In *2010 Proceedings IEEE INFOCOM*, pages 1–9, mar 2010. ISSN: 0743-166X.
- [49] Dimitris Bertsimas, Vivek F Farias, and Nikolaos Trichakis. The price of fairness. *Operations research*, 59(1):17–31, 2011.
- [50] Martin Abadi, Andy Chu, Ian Goodfellow, H. Brendan McMahan, Ilya Mironov, Kunal Talwar, and Li Zhang. Deep learning with differential privacy. In *Proceedings of the 2016 ACM SIGSAC Conference on Computer and Communications Security*, 2016.
- [51] Jinwen Ma, Lei Xu, and Michael I. Jordan. Asymptotic convergence rate of the em algorithm for gaussian mixtures. *Neural Computation*, 2000.
- [52] Elad Hoffer, Tal Ben-Nun, Itay Hubara, Niv Giladi, Torsten Hoefer, and Daniel Soudry. Augment your batch: better training with larger batches, 2019.
- [53] Li Deng. The mnist database of handwritten digit images for machine learning research [best of the web]. *IEEE Signal Processing Magazine*, 2012.
- [54] Han Xiao, Kashif Rasul, and Roland Vollgraf. Fashion-mnist: a novel image dataset for benchmarking machine learning algorithms. *CoRR*, 2017.

- [55] Alex Krizhevsky. Learning multiple layers of features from tiny images, 2009.
- [56] Peter Kairouz, H Brendan McMahan, Brendan Avent, Aurélien Bellet, Mehdi Bennis, Arjun Nitin Bhagoji, Kallista Bonawitz, Zachary Charles, Graham Cormode, Rachel Cummings, et al. Advances and open problems in federated learning. *Foundations and trends® in machine learning*, 14(1–2):1–210, 2021.
- [57] Maxence Noble, Aurélien Bellet, and Aymeric Dieuleveut. Differentially private federated learning on heterogeneous data. In *International Conference on Artificial Intelligence and Statistics*, 2021.
- [58] Cuong Tran, My-Hoa Nathalie Dinh, and Ferdinando Fioretto. Differentially private empirical risk minimization under the fairness lens. In *Neural Information Processing Systems*, 2021.
- [59] Allison Koenecke, Andrew Nam, Emily Lake, Joe Nudell, Minnie Quartey, Zion Mengesha, Connor Touns, John R Rickford, Dan Jurafsky, and Sharad Goel. Racial disparities in automated speech recognition. *Proceedings of the National Academy of Sciences*, 117(14):7684–7689, 2020.
- [60] Kaiming He, X. Zhang, Shaoqing Ren, and Jian Sun. Deep residual learning for image recognition. In *2016 IEEE Conference on Computer Vision and Pattern Recognition (CVPR)*, 2015.

Appendix for *Mitigating Disparate Impact of Differential Privacy in Federated Learning through Robust Clustering*

A Experimental setup

A.1 Datasets

Data split: We use three datasets MNIST, FMNIST and CIFAR10, and consider a distributed setting with 21 clients. In order to create majority and minority clusters, we consider 4 clusters with different number of clients $\{3, 6, 6, 6\}$ (21 clients in total). The first cluster with the minimum number of clients is the minority cluster, and the last three are the majority ones. The data belonging to the clients in each cluster has a different distribution $P(x, y)$ than that of the other clients with different clusters. We use two methods for making such data heterogeneity: 1. **covariate shift** 2. **concept shift**. In covariate shift we assume that data points marginal distribution $P(x)$ differs from one cluster to another cluster. In order to create such a data heterogeneity, we first allocate samples to all clients in an *uniform* way. Then we rotate the data points (images) belonging to the clients in cluster k by $k * 90$ degrees. For concept shift, we assume that conditional distribution $P(y|x)$ differs from one cluster to another cluster, and to simulate it, we first allocate images to clients in a uniform way, and flip the labels of the points allocated to clients: we flip $y_{i,j}$ (label of the j -th data point of client i , which belongs to cluster k) to $(y_{i,j} + k) \bmod 10$. The local datasets are balanced—all users have the same amount of training samples. The local data is split into train and test sets with ratios 80%, and 20%, respectively. In the reported experimental results, all users participate in each communication round.

Table 1: CNN model for classification on MNIST/FMNIST datasets

Layer	Output Shape	# of Trainable Parameters	Activation	Hyper-parameters
Input	(1, 28, 28)	0		
Conv2d	(16, 28, 28)	416	ReLU	kernel size =5; strides=(1, 1)
MaxPool2d	(16, 14, 14)	0		pool size=(2, 2)
Conv2d	(32, 14, 14)	12,832	ReLU	kernel size =5; strides=(1, 1)
MaxPool2d	(32, 7, 7)	0		pool size=(2, 2)
Flatten	1568	0		
Dense	10	15,690	ReLU	
Total		28,938		

A.1.1 Models:

We use a simple 2-layer CNN model with ReLU activation, the detail of which can be found in Table 1 for MNIST and FMNIST. To update the local models at each user using its local data, unless otherwise is stated, we apply stochastic gradient descent (SGD). Also, we use the residual neural network (ResNet-18) defined in [60], which is a large model. To update the local models at each client using its local data, we apply stochastic gradient descent (SGD).

Table 2: Details of the experiments and the used datasets in the main body of the paper. ResNet-18 is the residual neural networks defined in [60]. CNN: Convolutional Neural Network defined in Table 1.

Datasets	Train set size	Test set size	Data Partition method	# of clients	Model	# of parameters
MNIST	48000	12000	cov. shift [37]	$\{3, 6, 6, 6\}$	CNN	28,938
FMNIST	50000	10000	cov. shift [37]	$\{3, 6, 6, 6\}$	CNN	28,938
CIFAR10	50000	10000	cov. and con. shift [37]	$\{3, 6, 6, 6\}$	ResNet-18 [60]	11,181,642

B Proofs

Lemma 4.1. *Using the notations in Section 3, lets assume $\theta_{i,0}^e$ is the model parameter that is passed by the server to client i at the beginning of the round e , and it performs K local epochs of DPSGD on its local data \mathcal{D}_i with batch size b_i^e to generate the noisy DP model update $\Delta\tilde{\theta}_i^e(b_i^e)$. Assuming that the clipping threshold c is effective for all sampled data points in the batch, i.e. $\forall j \in \mathcal{B}_i^{e,t} : c < \|g_{ij}(\theta)\| = \|\nabla\ell(h(x_{ij}, \theta), y_{ij})\|$, we have:*

$$\sigma_i^{e,2}(b_i^e) := \text{Var}(\Delta\tilde{\theta}_i^e(b_i^e)|\theta_{i,0}^e) \approx K \cdot N_i \cdot \eta_i^2 \cdot \frac{pc^2 z^2(\epsilon, \delta, b_i^1, b_i^{>1}, N_i, K, E)}{b_i^{e,3}}. \quad (2)$$

Proof. We have assumed that the clipping threshold c is effective for all samples in the batch. Also, we know that the two sources of randomness (i.e. minibatch sampling and Gaussian noise) are independent, thus the variance is additive. Assuming that $E[\bar{g}_{ij}(\theta)]$ is the same for all j and is $G_i(\theta)$, we have:

$$\mathbb{E}[\tilde{g}_i^{e,t}(\theta)] = \frac{1}{b_i^e} \sum_{j \in \mathcal{B}_i^{e,t}} \mathbb{E}[\bar{g}_{ij}(\theta)] = \frac{1}{b_i^e} \sum_{j \in \mathcal{B}_i^{e,t}} G_i(\theta) = G_i(\theta). \quad (6)$$

We also have:

$$\begin{aligned} \sigma_{i,\bar{g}}^2(b_i^e) &:= \text{Var}(\tilde{g}_i^{e,t}(\theta)) = \text{Var}\left(\frac{1}{b_i^e} \sum_{j \in \mathcal{B}_i^{e,t}} \bar{g}_{ij}(\theta)\right) + \frac{p\sigma_{i,\text{DP}}^2}{b_i^{e,2}} \\ &= \frac{1}{b_i^{e,2}} \left(\mathbb{E}\left[\left\|\sum_{j \in \mathcal{B}_i^{e,t}} \bar{g}_{ij}(\theta)\right\|^2\right] - \left\|\mathbb{E}\left[\sum_{j \in \mathcal{B}_i^{e,t}} \bar{g}_{ij}(\theta)\right]\right\|^2 \right) + \frac{pc^2 z^2(\epsilon_i, \delta_i, b_i^1, b_i^{>1}, N_i, K, E)}{b_i^{e,2}} \\ &= \frac{1}{b_i^{e,2}} \left(\mathbb{E}\left[\left\|\sum_{j \in \mathcal{B}_i^{e,t}} \bar{g}_{ij}(\theta)\right\|^2\right] - \left\|\sum_{j \in \mathcal{B}_i^{e,t}} G_i(\theta)\right\|^2 \right) + \frac{pc^2 z^2(\epsilon_i, \delta_i, b_i^1, b_i^{>1}, N_i, K, E)}{b_i^{e,2}} \\ &= \frac{1}{b_i^{e,2}} \left(\underbrace{\mathbb{E}\left[\left\|\sum_{j \in \mathcal{B}_i^{e,t}} \bar{g}_{ij}(\theta)\right\|^2\right]}_{\mathcal{A}} - b_i^{e,2} \|G_i(\theta)\|^2 \right) + \frac{pc^2 z^2(\epsilon_i, \delta_i, b_i^1, b_i^{>1}, N_i, K, E)}{b_i^{e,2}}, \quad (7) \end{aligned}$$

where:

$$\begin{aligned} \mathcal{A} &= \mathbb{E}\left[\left\|\sum_{j \in \mathcal{B}_i^{e,t}} \bar{g}_{ij}(\theta)\right\|^2\right] = \sum_{j \in \mathcal{B}_i^{e,t}} \mathbb{E}\left[\|\bar{g}_{ij}(\theta)\|^2\right] + \sum_{m \neq n \in \mathcal{B}_i^{e,t}} 2\mathbb{E}\left[\bar{g}_{im}(\theta)^\top \bar{g}_{in}(\theta)\right] \\ &= \sum_{j \in \mathcal{B}_i^{e,t}} \mathbb{E}\left[\|\bar{g}_{ij}(\theta)\|^2\right] + \sum_{m \neq n \in \mathcal{B}_i^{e,t}} 2\mathbb{E}\left[\bar{g}_{im}(\theta)\right]^\top \mathbb{E}\left[\bar{g}_{in}(\theta)\right] \\ &= b_i^e c^2 + 2 \binom{b_i^e}{2} \|G_i(\theta)\|^2. \quad (8) \end{aligned}$$

The last equation has used Equation (6) and that we clip the norm of sample gradients $\bar{g}_{ij}(\theta)$ with an "effective" clipping threshold c . By replacing \mathcal{A} into eq. 7, we can rewrite it as:

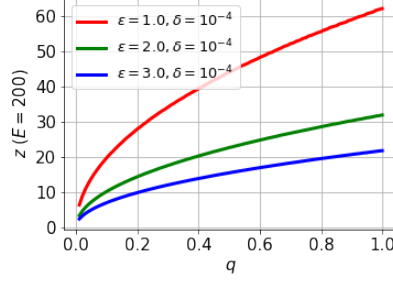


Figure 5: Plot of z v.s. q obtained from Moments Accountant [50] in a centralized setting with $E = 200$.

$$\begin{aligned}
\sigma_{i,\bar{g}}^2(b_i^e) &:= \text{Var}(\tilde{g}_i^{e,t}(\boldsymbol{\theta})) = \frac{1}{b_i^{e^2}} \left(\mathbb{E} \left[\left\| \sum_{j \in \mathcal{B}_i^{e,t}} \bar{g}_{ij}(\boldsymbol{\theta}) \right\|^2 \right] - b_i^{e^2} \|G_i(\boldsymbol{\theta})\|^2 \right) + \frac{pc^2 z^2(\epsilon_i, \delta_i, b_i^1, b_i^{>1}, N_i, K, E)}{b_i^{e^2}} \\
&= \frac{1}{b_i^{e^2}} \left(b_i^e c^2 + \left(2 \binom{b_i^e}{2} - b_i^{e^2} \right) \|G_i(\boldsymbol{\theta})\|^2 \right) + \frac{pc^2 z^2(\epsilon_i, \delta_i, b_i^1, b_i^{>1}, N_i, K, E)}{b_i^{e^2}} \\
&= \frac{c^2 - \|G_i(\boldsymbol{\theta})\|^2}{b_i^e} + \frac{pc^2 z^2(\epsilon_i, \delta_i, b_i^1, b_i^{>1}, N_i, K, E)}{b_i^{e^2}} \approx \frac{pc^2 z^2(\epsilon_i, \delta_i, b_i^1, b_i^{>1}, N_i, K, E)}{b_i^{e^2}}
\end{aligned} \tag{9}$$

The last approximation is valid because $p \gg 1$ (it is the number of model parameters).

Even when the clipping is ineffective for all samples, i.e. $\forall j \in \mathcal{B}_i^{e,t} : c > \|g_{ij}(\boldsymbol{\theta})\| = \|\nabla \ell(h(x_{ij}, \boldsymbol{\theta}), y_{ij})\|$, we have a noisy version of the batch gradient $g_i^{e,t}(\boldsymbol{\theta}) = \frac{1}{b_i^e} \sum_{j \in \mathcal{B}_i^{e,t}} g_{ij}(\boldsymbol{\theta})$, which is unbiased with variance bounded by $\sigma_{i,g}^2(b_i^e)$ (see Assumption 3.1). We note that $\sigma_{i,g}^2(b_i^e)$ is a constant that depends on the used batch size b_i^e . The larger the batch size b_i^e used during round e , the smaller the constant. Hence, in this case:

$$\mathbb{E}[\tilde{g}_i^{e,t}(\boldsymbol{\theta})] = \mathbb{E}[g_i^{e,t}(\boldsymbol{\theta})] = \nabla f_i(\boldsymbol{\theta}), \tag{10}$$

and

$$\begin{aligned}
\sigma_{i,\bar{g}}^2(b_i^e) &= \text{Var}(\tilde{g}_i^{e,t}(\boldsymbol{\theta})) = \text{Var}(g_i^{e,t}(\boldsymbol{\theta})) + \frac{p\sigma_{i,DP}^2}{b_i^{e^2}} \leq \sigma_{i,g}^2(b_i^e) + \frac{pc^2 z^2(\epsilon, \delta, b_i^1, b_i^{>1}, N_i, K, E)}{b_i^{e^2}} \\
&\approx \frac{pc^2 z^2(\epsilon, \delta, b_i^1, b_i^{>1}, N_i, K, E)}{b_i^{e^2}}.
\end{aligned} \tag{11}$$

In the equations above, we note that: 1. $\sigma_{i,g}^2(b_i^e)$ decreases with b_i^e . 2. z grows with b_i^1 and $b_i^{>1}$ sub-linearly (see Figure 5). Also, again the approximation is valid because $p \gg 1$ (number of model parameters). Therefore, $\sigma_{i,\bar{g}}^2(b_i^e)$, which is the variance of the client i 's DP batch gradients during communication round e , decreases with b_i^e fast. The lower the batch size of a client during round e , the larger the noise existing in its batch gradients during the round for the same level of privacy.

With the findings above, we now investigate the effect of batch size b_i^e on the noise level in clients' model updates at the end of round e . During the global communication round e , a participating client i performs $E_i(b_i^e) = K_i \cdot \lceil \frac{N_i}{b_i^e} \rceil$ batch gradient updates locally with step size η_i :

$$\begin{aligned}
\Delta \tilde{\boldsymbol{\theta}}_i^e &= \boldsymbol{\theta}_{i,E_i(b_i^e)}^e - \boldsymbol{\theta}_{i,0}^e, \\
\boldsymbol{\theta}_{i,k}^e &= \boldsymbol{\theta}_{i,k-1}^e - \eta_i \tilde{g}_i(\boldsymbol{\theta}_{i,k-1}^e), \quad k = 1, \dots, E_i(b_i^e).
\end{aligned} \tag{12}$$

In each update, it adds a Gaussian noise from $\mathcal{N}(0, \frac{c^2 z^2(\epsilon, \delta, b^1, b_i^{>1}, N_i, K, E)}{b_i^2} \mathbb{I}_p)$ to its batch gradients independently (see Equation (1)). Hence:

$$\sigma_i^{e^2} = \text{Var}(\Delta \tilde{\theta}_i^e | \theta_{i,0}^e) = K \cdot \lceil \frac{N_i}{b_i^e} \rceil \cdot \eta_i^2 \cdot \sigma_{i,\tilde{g}}^2(b_i^e), \quad (13)$$

where $\sigma_{i,\tilde{g}}^2(b_i^e)$ was computed in Equation (11), and was a decreasing function of b_i^e . Therefore:

$$\sigma_i^{e^2} = \text{Var}(\Delta \tilde{\theta}_i^e | \theta_{i,0}^e) \approx K \cdot N_i \cdot \eta_i^2 \cdot \frac{pc^2 z^2(\epsilon, \delta, b_i^1, b_i^{>1}, N_i, K, E)}{b_i^{e^3}}. \quad (14)$$

□

C Effect of batch size increment on clustering

Lemma 4.2. *Using the notations above, let's assume $\Delta_{m,m'}(b^1) := \|\mu_m^*(b^1) - \mu_{m'}^*(b^1)\|$ when $\forall i : b_i^1 = b^1$ (m and m' are two of the M Gaussian components). Then, the overlap between the pair of corresponding true Gaussian components $\mathcal{N}(\mu_m^*(b^1), \Sigma_m^*(b^1))$ and $\mathcal{N}(\mu_{m'}^*(b^1), \Sigma_{m'}^*(b^1))$ is $2Q(\frac{\sqrt{p}\Delta_{m,m'}(b^1)}{2\sigma^1(b^1)})$, where $\sigma^1(b^1) = \text{Var}(\Delta \tilde{\theta}_i^1 | \theta^{init}, b_i^1 = b^1)$ and $Q(\cdot)$ is the tail distribution function of the standard normal distribution. Furthermore, if we increase $b_i^1 = b^1$ to $b_i^1 = kb^1$ (for all i), the overlap between the corresponding components m and m' drops to $2Q(\frac{\sqrt{kp}\Delta_{m,m'}(b^1)}{2\sigma^1(b^1)})$.*

Proof. We first find the overlap between two arbitrary Gaussian distributions. Without loss of generality, let's assume we are in 1-dimensional space and that we have two Gaussian distributions both with variance σ^2 and with means $\mu_1 = 0$ and $\mu_2 = \mu$ ($\|\mu_1 - \mu_2\| = \mu$), respectively. Based on symmetry of the distributions, the two components start to overlap at $x = \frac{\mu}{2}$. Hence, we can find the overlap between the two gaussians as follows:

$$O := 2 \int_{\frac{\mu}{2}}^{\infty} \frac{1}{\sqrt{2\pi}\sigma} e^{-\frac{x^2}{2\sigma^2}} dx = 2 \int_{\frac{\mu}{2\sigma}}^{\infty} \frac{1}{\sqrt{2\pi}} e^{-\frac{x^2}{2}} dx = 2Q\left(\frac{\mu}{2\sigma}\right), \quad (15)$$

where $Q(\cdot)$ is the tail distribution function of the standard normal distribution. Now, let's consider the 2-dimensional space, and consider two similar symmetric distributions centered at $\mu_1 = (0, 0)$ and $\mu_2 = (\mu, 0)$ ($\|\mu_1 - \mu_2\| = \mu$) and with $\Sigma_1 = \Sigma_2 = \begin{bmatrix} \sigma^2 & 0 \\ 0 & \sigma^2 \end{bmatrix}$. The overlap between the two gaussians can be found as:

$$O = 2 \int_{-\infty}^{\infty} \int_{\frac{\mu}{2}}^{\infty} \frac{1}{2\pi\sigma^2} e^{-\frac{x^2+y^2}{2\sigma^2}} dx dy = 2 \int_{\frac{\mu}{2}}^{\infty} \frac{1}{\sqrt{2\pi}\sigma} e^{-\frac{x^2}{2\sigma^2}} dx \cdot \int_{-\infty}^{\infty} \frac{1}{\sqrt{2\pi}\sigma} e^{-\frac{y^2}{2\sigma^2}} dy = 2Q\left(\frac{\mu}{2\sigma}\right). \quad (16)$$

If we compute the overlap for two similar symmetric p -dimensional distributions with $\|\mu_1 - \mu_2\| = \mu$ and variance σ^2 in every direction, we will get to the same result $2Q(\frac{\mu}{2\sigma})$.

In the lemma, when using batch size b^1 , we have two Gaussian distributions $\mathcal{N}(\mu_m^*(b^1), \Sigma_m^*(b^1))$ and $\mathcal{N}(\mu_{m'}^*(b^1), \Sigma_{m'}^*(b^1))$, where

$$\Sigma_m^*(b^1) = \Sigma_{m'}^*(b^1) = \begin{bmatrix} \frac{\sigma^{1^2}(b^1)}{p} & & \\ & \ddots & \\ & & \frac{\sigma^{1^2}(b^1)}{p} \end{bmatrix}. \quad (17)$$

Therefore, from Equation (16), we can immediately conclude that the overlap between the two Gaussians, which we denote with $O_{m,m'}(b^1)$, is:

$$O_{m,m'}(b^1) = 2Q\left(\frac{\sqrt{p}\Delta_{m,m'}(b^1)}{2\sigma^1(b^1)}\right), \quad (18)$$

which proves the first part of the lemma.

Now, lets see the effect of increasing batch size. First, note that we had:

$$\begin{aligned} \Delta\tilde{\theta}_i^1 &= \theta_{i,E_i(b_i^e)}^1 - \theta_{i,0}^1, \\ \theta_{i,k}^1 &= \theta_{i,k-1}^1 - \eta_l \tilde{g}_i(\theta_{i,k-1}^1), \quad k = 1, \dots, E_i(b^1), \end{aligned} \quad (19)$$

where $E_i(b^1) = K \cdot \lceil \frac{N}{b^1} \rceil$. Therefore, considering that DP batch gradients are clipped with a bound c , we have:

$$\|\mathbb{E}[\Delta\tilde{\theta}_i^1(b^1)]\| \leq E_i(b^1) \cdot \eta_l \cdot c. \quad (20)$$

The upperbound in Equation (20) gets k times smaller when we increase batch size b_i^1 for all clients from b^1 to kb^1 , i.e. the number of local gradient updates that each client performs during each round e decreases k times, and on average, its model update get at least k times smaller. As such, we can write:

$$\Delta\tilde{\theta}_i^1(b^1) = k \cdot \Delta\tilde{\theta}_i^1(kb^1) + v_i, \quad (21)$$

where $v_i \in \mathbb{R}^p$ is a random vector capturing the discrepancies between $\Delta\tilde{\theta}_i^1(b^1)$ and $k \cdot \Delta\tilde{\theta}_i^1(kb^1)$. Therefore, we have:

$$\begin{aligned} \mu_m^*(b^1) &= \mathbb{E}[\Delta\tilde{\theta}_i^1(b^1)|s(i) = m] = \mathbb{E}[k \cdot \Delta\tilde{\theta}_i^1(kb^1) + v_i|s(i) = m] \\ &= k \cdot \mathbb{E}[\Delta\tilde{\theta}_i^1(kb^1)] + \mathbb{E}[v_i|s(i) = m] = k \cdot \mu_m^*(kb^1) + \mathbb{E}[v_i|s(i) = m] \\ &\approx k \cdot \mu_m^*(kb^1). \end{aligned} \quad (22)$$

Based on our experiments, on average v_i has a small norm, and we can ignore it when analyzing the average case. Equivalently:

$$\|\mu_m^*(kb^1) - \mu_{m'}^*(kb^1)\| \approx \frac{\|\mu_m^*(b^1) - \mu_{m'}^*(b^1)\|}{k}. \quad (23)$$

On the other hand, from Equation (2), we have:

$$\forall m \in [M] : \sigma_m^2(b^1) = \sigma^2(b^1) \approx K \cdot N \cdot \eta_l^2 \cdot \frac{pc^2 z^2(\epsilon, \delta, b^1, b^{>1}, N, K, E)}{b^{1^3}}. \quad (24)$$

Now, when we change the batch size used during the first communication round $e = 1$ from b^1 to kb^1 (and we keep the batch size of rounds $e > 1$ as fixed), then the noise scale z changes from $z(\epsilon, \delta, b^1, b^{>1}, N_i, K, E)$ to $z(\epsilon, \delta, kb^1, b^{>1}, N_i, K, E)$. Confirmed from experiments, the amount of change in z due to this is very small, as we have changed the batch size only in the first round $e = 1$ from b^1 to kb^1 , while the batch sizes in the other $E - 1$ rounds are unchanged and $E \gg 1$. So we can redo the computation as;

$$\begin{aligned}
\forall m \in [M] : \sigma_m^2(kb^1) &= \sigma^2(kb^1) \approx K \cdot N \cdot \eta_l^2 \cdot \frac{pc^2 z^2(\epsilon, \delta, kb^1, b^{>1}, N, K, E)}{(kb^1)^3} \\
&\approx K \cdot N \cdot \eta_l^2 \cdot \frac{pc^2 z^2(\epsilon, \delta, b^1, b^{>1}, N, K, E)}{(kb^1)^3} \\
&= \frac{1}{k^3} \cdot \sigma^2(b^1). \tag{25}
\end{aligned}$$

From Equation (23) and Equation (25), we have:

$$\begin{aligned}
O_{m,m'}(kb^1) &= 2Q\left(\frac{\sqrt{p}\Delta_{m,m'}(kb^1)}{2\sigma(kb^1)}\right) \approx 2Q\left(\frac{\sqrt{p}\frac{\Delta_{m,m'}(b^1)}{k}}{2\frac{\sigma(b^1)}{k^{\frac{3}{2}}}}\right) = 2Q\left(\frac{\sqrt{p}k\Delta_{m,m'}(b^1)}{2\frac{\sigma(b^1)}{k^{\frac{3}{2}}}}\right) \\
&= 2Q\left(\frac{\sqrt{kp}\Delta_{m,m'}(b^1)}{2\sigma(b^1)}\right) \tag{26}
\end{aligned}$$

□

Theorem 4.3. ([51]) Given iid model updates $\{\Delta\tilde{\theta}_i^1(b^1)\}_{i=1}^n$ sampled from the mixture of Gaussians $\{\mathcal{N}(\mu_m^*(b^1), \Sigma_m^*(b^1)), \alpha_m^*\}_{m=1}^M$ that satisfies conditions 1 and 2, as b^1 grows. If b^1 grows enough that $O(\psi^*(b^1))$ is considered as an infinitesimal, we have:

$$\lim_{r \rightarrow \infty} \frac{\|\psi^{r+1} - \psi^*(b^1)\|}{\|\psi^r - \psi^*(b^1)\|} = o(O(\psi^*(b^1))^{0.5-\epsilon}), \tag{5}$$

as n grows, where ψ^r is the mixture model parameters returned by GMM after r iterations. ϵ is an arbitrary small positive number, and $o(x)$ means it is a higher order infinitesimal as $x \rightarrow 0$.

Proof. The proof directly follows from the proof of Theorem 1 in [51] by considering $\{\Delta\tilde{\theta}_i^1(b^1)\}_{i=1}^n$ as the samples of Gaussian mixture $\{\mathcal{N}(\mu_m^*(b^1), \Sigma_m^*(b^1)), \alpha_m^*\}_{m=1}^M$. □

D Detailed experimental results

D.1 MNIST data split with covariate shift

Table 3: Average test accuracy of all (All), majority (Maj) and minority (Min) clients on the split of MNIST dataset with covariate shift (rotation). The results are averaged over 3 seeds.

algorithm		$\epsilon = 10$	$\epsilon = 5$	$\epsilon = 4$	$\epsilon = 3$	$\epsilon = 2$	
MNIST	DPFedAvg	All:	80.92 \pm 0.83	79.37 \pm 0.76	78.73 \pm 1.04	72.88 \pm 0.79	72.29 \pm 0.77
		Maj:	82.47 \pm 0.01	81.16 \pm 0.01	80.35 \pm 0.05	75.45 \pm 0.02	75.02 \pm 0.05
		Min:	67.16 \pm 1.37	64.04 \pm 2.06	63.29 \pm 1.83	52.80 \pm 2.24	52.50 \pm 2.76
	f-CDPFL	All:	90.64 \pm 1.45	89.12 \pm 1.69	87.75 \pm 0.99	84.56 \pm 3.91	85.01 \pm 2.71
		Maj:	92.72 \pm 1.42	91.25 \pm 0.01	85.93 \pm 0.02	81.75 \pm 0.3	88.80 \pm 0.03
		Min:	86.98 \pm 5.77	79.12 \pm 8.94	81.36 \pm 6.03	88.12 \pm 1.02	76.07 \pm 17.79
	KM-CDPFL	All:	81.42 \pm 3.03	77.80 \pm 0.47	77.40 \pm 2.06	71.91 \pm 2.29	68.89 \pm 1.20
		Maj:	81.55 \pm 0.01	79.20 \pm 0.01	80.60 \pm 0.07	74.38 \pm 0.02	73.11 \pm 0.02
		Min:	78.78 \pm 0.08	59.01 \pm 5.07	52.57 \pm 9.51	42.33 \pm 5.2	35.13 \pm 1.81
	RC-DPFL	All:	92.28 \pm 0.40	90.7 \pm 0.47	89.89 \pm 0.43	89.00 \pm 0.44	87.92 \pm 0.36
		Maj:	92.06 \pm 0.01	90.63 \pm 1.42	89.95 \pm 0.01	88.78 \pm 0.02	87.76 \pm 0.03
		Min:	90.45 \pm 0.19	89.33 \pm 0.24	87.44 \pm 0.54	88.21 \pm 0.67	85.83 \pm 0.26
Oracle-CDPFL	All:	92.71 \pm 0.27	91.06 \pm 0.06	91.09 \pm 0.53	89.33 \pm 0.44	88.94 \pm 0.47	
	Maj:	92.70 \pm 0.01	91.10 \pm 0.03	90.91 \pm 0.02	89.10 \pm 0.05	88.71 \pm 1.42	
	Min:	91.11 \pm 0.25	90.28 \pm 0.02	89.87 \pm 0.46	89.10 \pm 0.089	88.23 \pm 0.52	

Table 4: Fairness evaluation in terms of different metrics on the split of MNIST dataset with covariate shift (rotation). The results are averaged over 3 seeds.

algorithm		$\epsilon = 10$	$\epsilon = 5$	$\epsilon = 4$	$\epsilon = 3$	$\epsilon = 2$	
MNIST	DPFedAvg	\mathcal{F}_{acc} :	18.41 \pm 0.80	20.81 \pm 2.18	20.74 \pm 1.46	27.93 \pm 1.68	27.57 \pm 1.89
		\mathcal{F}_{loss} :	1.18 \pm 0.16	1.49 \pm 0.26	1.54 \pm 0.25	1.53 \pm 0.36	1.61 \pm 0.32
		Min Acc:	66.33 \pm 1.28	63.26 \pm 2.25	62.58 \pm 2.20	51.55 \pm 2.88	51.46 \pm 3.04
		Accuracy Disparity:	18.56 \pm 0.57	21.06 \pm 2.26	21.00 \pm 1.50	28.25 \pm 1.75	27.93 \pm 1.87
	f-CDPFL	\mathcal{F}_{acc} :	8.70 \pm 5.52	13.39 \pm 9.28	13.60 \pm 3.07	10.15 \pm 5.75	17.81 \pm 15.77
		\mathcal{F}_{loss} :	0.60 \pm 0.21	0.81 \pm 0.19	0.86 \pm 0.11	0.57 \pm 0.11	0.89 \pm 0.17
		Min Acc:	84.81 \pm 4.98	78.76 \pm 9.02	78.25 \pm 2.71	79.75 \pm 6.44	72.20 \pm 15.79
		Accuracy Disparity:	9.05 \pm 5.33	13.70 \pm 9.12	13.83 \pm 3.07	10.21 \pm 5.70	17.88 \pm 15.70
	KM-CDPFL	\mathcal{F}_{acc} :	18.67 \pm 6.54	41.43 \pm 10.58	46.69 \pm 9.40	46.68 \pm 4.56	54.17 \pm 2.67
		\mathcal{F}_{loss} :	1.48 \pm 0.31	2.73 \pm 0.24	3.33 \pm 0.23	2.33 \pm 0.24	3.26 \pm 0.58
		Min Acc:	73.33 \pm 6.95	48.66 \pm 10.04	43.71 \pm 9.25	40.58 \pm 5.24	32.86 \pm 2.57
		Accuracy Disparity:	18.81 \pm 6.45	41.58 \pm 10.67	47.08 \pm 9.58	46.98 \pm 4.43	54.48 \pm 2.69
	RC-DPFL	\mathcal{F}_{acc} :	4.04 \pm 0.90	3.13 \pm 0.36	4.27 \pm 0.80	2.95 \pm 0.84	4.40 \pm 1.22
		\mathcal{F}_{loss} :	0.55 \pm 0.15	0.46 \pm 0.16	0.68 \pm 0.06	0.35 \pm 0.14	0.52 \pm 0.15
		Min Acc:	89.46 \pm 0.28	88.71 \pm 0.14	86.91 \pm 0.52	87.43 \pm 0.81	85.23 \pm 0.54
		Accuracy Disparity:	4.41 \pm 0.81	3.36 \pm 0.23	4.53 \pm 0.59	2.99 \pm 0.64	4.48 \pm 1.00
Oracle-CDPFL	\mathcal{F}_{acc} :	3.35 \pm 0.81	3.10 \pm 0.73	2.93 \pm 0.49	2.92 \pm 0.75	2.85 \pm 0.66	
	\mathcal{F}_{loss} :	0.43 \pm 0.12	0.36 \pm 0.08	0.43 \pm 0.08	0.32 \pm 0.05	0.36 \pm 0.08	
	Min Acc:	90.33 \pm 0.45	89.36 \pm 0.37	89.13 \pm 0.28	87.73 \pm 0.81	87.43 \pm 0.86	
	Accuracy Disparity:	3.71 \pm 0.79	3.13 \pm 0.51	3.21 \pm 0.38	2.91 \pm 0.74	2.93 \pm 0.47	

D.2 FMNIST data split with covariate shift

Table 5: Average test accuracy of all (All), majority (Maj) and minority (Min) clients on the split of FMNIST dataset with covariate shift (rotation). The results are averaged over 3 seeds.

algorithm		$\epsilon = 10$	$\epsilon = 5$	$\epsilon = 4$	$\epsilon = 3$	$\epsilon = 2$	
FMNIST	DPFedAvg	All:	62.62 \pm 0.39	62.22 \pm 0.35	62.32 \pm 0.93	59.58 \pm 0.25	59.78 \pm 0.25
		Maj:	66.27 \pm 0.05	65.86 \pm 0.05	65.86 \pm 0.03	62.90 \pm 7.10	62.96 \pm 0.03
		Min:	42.32 \pm 1.55	41.61 \pm 1.18	44.84 \pm 6.62	38.15 \pm 0.73	43.23 \pm 3.91
	f-CDPFL	All:	78.19 \pm 1.53	74.37 \pm 0.46	75.26 \pm 2.38	70.10 \pm 1.30	70.42 \pm 3.84
		Maj:	76.12 \pm 0.05	73.43 \pm 0.03	72.48 \pm 0.03	67.82 \pm 0.04	67.35 \pm 0.06
		Min:	76.21 \pm 4.92	73.43 \pm 6.62	77.89\pm0.96	69.85\pm7.48	69.88 \pm 7.63
	KM-CDPFL	All:	60.17 \pm 2.15	57.65 \pm 1.09	57.34 \pm 0.19	54.82 \pm 2.95	53.55 \pm 0.47
		Maj:	57.79 \pm 0.02	58.75 \pm 0.03	63.22 \pm 7.10	53.31 \pm 0.03	58.30 \pm 0.06
		Min:	59.81 \pm 4.34	31.72 \pm 20.48	15.95 \pm 2.90	32.33 \pm 2.78	19.70 \pm 7.14
	RC-DPFL	All:	80.26\pm0.22	78.15\pm0.23	77.80\pm0.50	74.04\pm1.54	74.84\pm0.43
		Maj:	80.50\pm0.02	78.41\pm0.02	78.12\pm0.06	75.11\pm0.06	74.93\pm0.04
		Min:	79.03\pm1.57	77.23\pm1.30	76.21 \pm 1.96	69.35 \pm 7.17	73.29\pm1.55
	Oracle-CDPFL	All:	80.46 \pm 0.10	78.44 \pm 0.18	78.31 \pm 0.22	75.19 \pm 0.16	75.11 \pm 0.17
		Maj:	80.76 \pm 0.02	78.42 \pm 0.03	78.31 \pm 0.3	75.02 \pm 0.05	75.21 \pm 0.03
		Min:	79.76 \pm 0.96	78.35 \pm 0.62	77.81 \pm 1.02	75.33 \pm 0.53	75.00 \pm 1.01

Table 6: Fairness evaluation in terms of different metrics on the split of FMNIST dataset with covariate shift (rotation). The results are averaged over 3 seeds.

algorithm		$\epsilon = 10$	$\epsilon = 5$	$\epsilon = 4$	$\epsilon = 3$	$\epsilon = 2$	
FMNIST	DPFedAvg	\mathcal{F}_{acc} :	25.07 \pm 2.16	24.86 \pm 1.44	23.31 \pm 6.22	26.53 \pm 2.35	22.97 \pm 4.59
		\mathcal{F}_{loss} :	1.26 \pm 0.05	1.02 \pm 0.08	0.99 \pm 0.24	0.83 \pm 0.08	0.77 \pm 0.18
		Min Acc:	41.60 \pm 1.55	40.69 \pm 1.34	43.93 \pm 6.45	37.30 \pm 1.02	42.22 \pm 4.08
		Accuracy Disparity:	27.86 \pm 0.98	28.11 \pm 1.27	25.83 \pm 5.02	29.58 \pm 0.70	25.12 \pm 3.31
	f-CDPFL	\mathcal{F}_{acc} :	11.59 \pm 1.16	11.43 \pm 1.22	12.00 \pm 0.80	18.13 \pm 2.15	12.87 \pm 1.59
		\mathcal{F}_{loss} :	0.32 \pm 0.09	0.33 \pm 0.05	0.37 \pm 0.03	0.42 \pm 0.07	0.33 \pm 0.04
		Min Acc:	72.31 \pm 4.33	66.73 \pm 2.89	70.61 \pm 4.12	61.19 \pm 2.26	64.93 \pm 6.69
		Accuracy Disparity:	9.36 \pm 4.22	13.11 \pm 2.64	9.60 \pm 3.85	15.08 \pm 2.01	11.08 \pm 4.86
	KM-CDPFL	\mathcal{F}_{acc} :	43.55 \pm 2.16	59.20 \pm 6.77	63.41 \pm 1.25	48.46 \pm 4.18	54.50 \pm 6.54
		\mathcal{F}_{loss} :	2.44 \pm 0.25	3.36 \pm 0.99	3.33 \pm 0.35	1.89 \pm 0.42	2.28 \pm 0.40
		Min Acc:	33.33 \pm 2.08	12.41 \pm 7.07	9.66 \pm 0.23	21.03 \pm 2.39	14.03 \pm 7.47
		Accuracy Disparity:	43.83 \pm 2.48	62.78 \pm 7.73	66.08 \pm 0.87	51.40 \pm 2.53	57.91 \pm 8.10
	RC-DPFL	\mathcal{F}_{acc} :	7.37\pm2.70	7.25\pm3.29	7.73\pm2.95	10.55\pm5.18	6.92\pm2.69
		\mathcal{F}_{loss} :	0.28\pm0.06	0.24\pm0.05	0.30\pm0.08	0.22\pm0.07	0.27\pm0.02
		Min Acc:	77.31\pm1.07	75.16\pm1.04	74.03\pm1.29	67.66\pm6.64	71.76\pm1.62
		Accuracy Disparity:	5.18\pm1.43	5.5\pm1.14	6.46\pm1.10	9.21\pm6.10	5.66\pm1.29
Oracle-CDPFL	\mathcal{F}_{acc} :	7.37 \pm 2.90	6.27 \pm 2.96	6.50 \pm 3.19	6.51 \pm 3.01	6.55 \pm 3.41	
	\mathcal{F}_{loss} :	0.24 \pm 0.03	0.24 \pm 0.07	0.24 \pm 0.06	0.20 \pm 0.08	0.20 \pm 0.08	
	Min Acc:	77.70 \pm 0.64	76.61 \pm 0.59	75.98 \pm 0.87	73.11 \pm 0.33	72.71 \pm 0.68	
	Accuracy Disparity:	5.05 \pm 1.32	3.91 \pm 0.49	4.61 \pm 0.77	4.08 \pm 0.02	4.75 \pm 0.35	

D.3 CIFAR10 data split with covariate shift

Table 7: Average test accuracy of all (All), majority (Maj) and minority (Min) clients on the split of CIFAR10 dataset with covariate shift (rotation). The results are averaged over 3 seeds.

algorithm		$\epsilon = 10$	$\epsilon = 5$	$\epsilon = 4$	$\epsilon = 3$	$\epsilon = 2$	
CIFAR10 (covariate shift)	DPFedAvg	All:	36.50 \pm 0.10	33.64 \pm 0.01	33.04 \pm 0.07	28.55 \pm 0.01	28.12 \pm 0.18
		Maj:	37.39 \pm 0.02	34.18 \pm 0.02	33.69 \pm 0.05	29.09 \pm 0.01	29.00 \pm 0.04
		Min:	32.10 \pm 0.03	30.03 \pm 0.14	29.68 \pm 0.15	25.84 \pm 0.24	25.48 \pm 0.47
	f-CDPFL	All:	40.20\pm0.50	35.72\pm0.01	35.16\pm0.01	30.38\pm0.21	29.17\pm0.07
		Maj:	41.00\pm0.04	36.62\pm0.02	36.03\pm0.05	30.81\pm0.08	30.05\pm0.11
		Min:	36.80 \pm 1.53	31.16 \pm 0.61	30.83 \pm 1.32	27.58 \pm 1.47	26.05 \pm 0.13
	KM-CDPFL	All:	34.86 \pm 0.23	31.46 \pm 0.12	30.48 \pm 0.84	26.48 \pm 0.01	26.10 \pm 0.08
		Maj:	36.05 \pm 0.12	32.47 \pm 0.15	32.02 \pm 0.04	27.16 \pm 0.01	26.79 \pm 0.12
		Min:	27.69 \pm 0.23	25.43 \pm 0.08	25.20 \pm 0.26	22.43 \pm 0.01	21.93 \pm 0.13
	RC-DPFL	All:	39.97 \pm 0.09	35.20 \pm 0.25	34.23 \pm 0.23	29.92 \pm 0.50	27.78 \pm 0.69
		Maj:	40.52 \pm 0.12	35.97 \pm 0.04	35.05 \pm 0.05	30.52 \pm 0.05	28.80 \pm 0.05
		Min:	37.75\pm0.10	32.76\pm0.26	32.26\pm0.54	27.85\pm1.12	26.13\pm0.05
	Oracle-CDPFL	All:	40.43 \pm 0.17	36.39 \pm 0.20	35.46 \pm 0.43	30.79 \pm 0.19	29.34 \pm 0.61
		Maj:	41.07 \pm 0.05	36.95 \pm 0.05	36.47 \pm 0.11	31.12 \pm 0.05	30.41 \pm 3.55
		Min:	37.84 \pm 0.32	34.49 \pm 0.33	33.07 \pm 0.39	29.63 \pm 0.76	27.38 \pm 1.12

Table 8: Fairness evaluation in terms of different metrics on the split of CIFAR10 dataset with covariate shift (rotation). The results are averaged over 3 seeds.

algorithm		$\epsilon = 10$	$\epsilon = 5$	$\epsilon = 4$	$\epsilon = 3$	$\epsilon = 2$	
CIFAR10 (covariate shift)	DPFedAvg	\mathcal{F}_{acc} :	9.31 \pm 0.76	9.32 \pm 1.06	9.81 \pm 0.59	9.13 \pm 2.13	9.11 \pm 2.15
		\mathcal{F}_{loss} :	0.16 \pm 0.01	0.14 \pm 0.01	0.12 \pm 0.01	0.08 \pm 0.01	0.07 \pm 0.01
		Min Acc:	31.65 \pm 0.02	28.81 \pm 0.05	28.45 \pm 0.28	24.79 \pm 0.19	24.65 \pm 0.33
		Accuracy Disparity:	8.57 \pm 0.17	8.14 \pm 0.45	8.09 \pm 1.10	7.63 \pm 0.81	7.07 \pm 0.33
	f-CDPFL	\mathcal{F}_{acc} :	7.53 \pm 0.73	6.90\pm0.53	7.09 \pm 0.75	7.11\pm1.36	7.61 \pm 0.9
		\mathcal{F}_{loss} :	0.16 \pm 0.04	0.19 \pm 0.02	0.18 \pm 0.05	0.12 \pm 0.01	0.09\pm0.02
		Min Acc:	35.97 \pm 1.47	30.31 \pm 0.56	29.75 \pm 0.76	27.43 \pm 1.04	25.01 \pm 0.93
		Accuracy Disparity:	7.71 \pm 1.50	8.29 \pm 1.13	8.57 \pm 0.76	5.55\pm1.30	6.89 \pm 1.52
	KM-CDPFL	\mathcal{F}_{acc} :	10.88 \pm 0.28	9.30 \pm 0.97	8.90 \pm 0.421	9.18 \pm 0.61	8.76 \pm 0.64
		\mathcal{F}_{loss} :	0.32 \pm 0.07	0.24 \pm 0.01	0.22 \pm 0.02	0.13 \pm 0.01	0.12 \pm 0.02
		Min Acc:	26.87 \pm 0.72	24.65 \pm 0.08	24.19 \pm 0.82	21.05 \pm 0.23	20.87 \pm 0.12
		Accuracy Disparity:	14.21 \pm 0.65	11.63 \pm 0.07	10.79 \pm 2.05	9.71 \pm 0.23	9.35 \pm 0.13
	RC-DPFL	\mathcal{F}_{acc} :	7.4\pm0.68	7.49 \pm 0.74	7.05\pm1.10	8.14 \pm 1.76	7.03\pm1.17
		\mathcal{F}_{loss} :	0.10\pm0.03	0.10\pm0.01	0.10\pm0.01	0.10\pm0.01	0.68 \pm 0.01
		Min Acc:	37.29\pm0.11	31.95\pm0.28	31.37\pm0.33	27.81\pm0.98	25.37\pm0.14
		Accuracy Disparity:	6.35\pm0.34	6.21\pm0.56	5.19\pm1.15	5.87 \pm 0.48	6.05\pm0.84
	Oracle-CDPFL	\mathcal{F}_{acc} :	7.08 \pm 0.46	7.53 \pm 0.61	7.43 \pm 0.72	6.89 \pm 0.07	6.62 \pm 0.28
		\mathcal{F}_{loss} :	0.10 \pm 0.02	0.09 \pm 0.01	0.10 \pm 0.02	0.07 \pm 0.01	0.08 \pm 0.01
		Min Acc:	37.41 \pm 0.39	33.29 \pm 0.42	31.91 \pm 0.16	28.25 \pm 0.76	26.13 \pm 0.98
		Accuracy Disparity:	6.69 \pm 0.28	5.29 \pm 0.22	6.25 \pm 0.53	4.63 \pm 0.65	5.75 \pm 0.25

D.4 CIFAR10 data split with concept shift

Table 9: Average test accuracy of all (All), majority (Maj) and minority (Min) clients on the split of CIFAR10 dataset with concept shift (label flip). The results are averaged over 3 seeds.

algorithm		$\epsilon = 10$	$\epsilon = 5$	$\epsilon = 4$	$\epsilon = 3$	$\epsilon = 2$	
CIFAR10 (concept shift)	DPFedAvg	All:	17.98 \pm 0.31	17.19 \pm 0.20	17.10 \pm 0.14	17.06 \pm 0.19	15.28 \pm 0.27
		Maj:	19.26 \pm 0.02	18.17 \pm 0.02	17.85 \pm 0.11	17.80 \pm 0.19	15.86 \pm 0.25
		Min:	12.51 \pm 0.58	12.86 \pm 0.32	12.56 \pm 0.43	12.65 \pm 0.40	11.55 \pm 0.88
	f-CDPFL	All:	35.27 \pm 2.83	33.21 \pm 0.26	31.74 \pm 1.56	29.70 \pm 1.84	25.18\pm1.32
		Maj:	35.12 \pm 3.30	33.56 \pm 0.02	32.42\pm0.92	30.11 \pm 2.22	25.89\pm0.65
		Min:	36.17\pm0.37	32.12 \pm 0.21	27.68 \pm 5.58	27.25\pm4.70	20.95\pm5.37
	KM-CDPFL	All:	19.67 \pm 0.70	17.80 \pm 0.30	17.98 \pm 0.58	17.70 \pm 0.67	15.50 \pm 0.30
		Maj:	20.95 \pm 0.72	19.49 \pm 0.03	19.27 \pm 0.65	18.99 \pm 0.80	16.44 \pm 0.30
		Min:	12.01 \pm 0.91	10.46 \pm 0.55	10.31 \pm 0.46	9.91 \pm 0.52	9.89 \pm 1.01
	RC-DPFL	All:	37.16\pm0.26	33.41\pm0.49	32.12\pm0.44	30.25\pm1.45	23.85 \pm 1.40
		Maj:	37.45\pm0.23	33.62\pm0.02	32.39 \pm 0.45	30.98\pm0.91	24.72 \pm 0.80
		Min:	35.38 \pm 0.44	32.22\pm0.60	30.54\pm0.51	25.90 \pm 4.70	18.61 \pm 5.20
	Oracle-CDPFL	All:	37.40 \pm 0.30	33.93 \pm 0.20	32.98 \pm 0.31	32.36 \pm 0.24	26.39 \pm 0.23
		Maj:	37.64 \pm 0.27	33.81 \pm 0.05	33.20 \pm 0.28	32.67 \pm 0.28	26.59 \pm 0.12
		Min:	35.98 \pm 0.56	32.91 \pm 0.28	31.65 \pm 0.45	30.56 \pm 0.12	25.16 \pm 0.88

Table 10: Fairness evaluation in terms of different metrics on the split of CIFAR10 dataset with concept shift (label flip). The results are averaged over 3 seeds.

algorithm		$\epsilon = 10$	$\epsilon = 5$	$\epsilon = 4$	$\epsilon = 3$	$\epsilon = 2$	
CIFAR10 (concept shift)	DPFedAvg	\mathcal{F}_{acc} :	12.14 \pm 0.92	9.25 \pm 1.55	10.03 \pm 1.38	9.59 \pm 2.26	8.59 \pm 0.99
		\mathcal{F}_{loss} :	0.29 \pm 0.01	0.24 \pm 0.03	0.21 \pm 0.02	0.20 \pm 0.01	0.13 \pm 0.02
		Min Acc:	11.11 \pm 0.45	11.63 \pm 0.25	11.19 \pm 0.31	11.55 \pm 0.76	11.17 \pm 0.86
		Accuracy Disparity:	11.89 \pm 0.27	9.49 \pm 0.05	10.53 \pm 1.06	9.83 \pm 1.62	6.95 \pm 1.82
	f-CDPFL	\mathcal{F}_{acc} :	11.40 \pm 4.66	8.38 \pm 0.34	9.44 \pm 1.13	11.54 \pm 5.45	9.54 \pm 0.98
		\mathcal{F}_{loss} :	0.14 \pm 0.07	0.08 \pm 0.01	0.16 \pm 0.12	0.22 \pm 0.09	0.09\pm0.05
		Min Acc:	32.15 \pm 4.49	31.07\pm0.17	26.69 \pm 5.44	23.45 \pm 4.48	19.97\pm5.13
		Accuracy Disparity:	7.33 \pm 4.44	4.26 \pm 0.17	8.45 \pm 5.56	11.01 \pm 4.73	8.59\pm5.34
	KM-CDPFL	\mathcal{F}_{acc} :	20.99 \pm 1.67	16.66 \pm 2.41	16.41 \pm 2.92	15.95 \pm 3.23	11.15 \pm 2.63
		\mathcal{F}_{loss} :	0.59 \pm 0.07	0.46 \pm 0.01	0.47 \pm 0.02	0.45 \pm 0.03	0.24 \pm 0.01
		Min Acc:	10.61 \pm 1.30	9.43 \pm 0.61	9.25 \pm 0.39	8.89 \pm 0.66	9.07 \pm 1.103
		Accuracy Disparity:	21.35 \pm 2.44	17.85 \pm 1.47	18.21 \pm 2.03	18.71 \pm 2.63	12.75 \pm 1.81
	RC-DPFL	\mathcal{F}_{acc} :	8.09\pm1.18	8.20\pm0.20	7.88\pm0.70	8.37\pm1.08	8.03\pm0.03
		\mathcal{F}_{loss} :	0.09\pm0.01	0.07\pm0.02	0.06\pm0.01	0.16\pm0.08	0.12 \pm 0.07
		Min Acc:	34.69\pm0.11	30.97 \pm 0.82	29.45\pm0.71	24.57\pm4.99	17.61 \pm 5.09
		Accuracy Disparity:	4.45\pm0.79	4.21\pm0.08	5.06\pm0.81	9.53\pm5.49	10.07 \pm 4.82
Oracle-CDPFL	\mathcal{F}_{acc} :	8.77 \pm 1.29	8.88 \pm 0.38	8.00 \pm 0.44	7.80 \pm 0.45	8.28 \pm 0.46	
	\mathcal{F}_{loss} :	0.09 \pm 0.01	0.07 \pm 0.01	0.06 \pm 0.01	0.08 \pm 0.01	0.05 \pm 0.01	
	Min Acc:	34.83 \pm 0.63	30.59 \pm 0.32	30.91 \pm 0.53	29.63 \pm 0.30	23.83 \pm 0.96	
	Accuracy Disparity:	4.97 \pm 0.88	4.91 \pm 0.22	4.49 \pm 0.21	5.17 \pm 0.51	5.17 \pm 0.96	

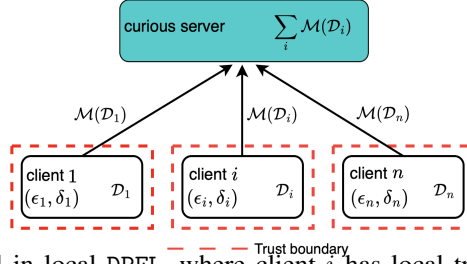


Figure 6: Security model in local DPFL, where client i has local train data \mathcal{D}_i and DP privacy parameters (ϵ_i, δ_i) , and does not trust any external parties. In this work, we assume uniform privacy parameters: $\forall i : (\epsilon_i, \delta_i) = (\epsilon, \delta)$.

E Gradient accumulation

When training large models with DPSGD, increasing the batch size results in memory exploding during training or finetuning. This might happen even when we are not using DP training. On the other hand, using a small batch size results in larger stochastic noise in batch gradients. Also, in the case of DP training, using a small batch size results in fast increment of DP noise (as explained in 4.1 in details). Therefore, if the memory budget of devices allow, we prefer to avoid using small batch sizes. But what if there is a limited memory budget? A solution for virtually increasing batch size is “gradient accumulation”, which is very useful when the available physical memory of GPU is insufficient to accommodate the desired batch size. In gradient accumulation, gradients are computed for smaller batch sizes and summed over multiple batches, instead of updating model parameters after computing each batch gradient. When the accumulated gradients reach the target logical batch size, the model weights are updated with the accumulated batch gradients. The page in https://opacus.ai/api/batch_memory_manager.html shows the implementation of gradient accumulation for DP training.

F Security model

We consider a uniform DPFL system with local differential privacy (LDP), as observed in Figure 6.